Effect of Mount Pinatubo H_2SO_4/H_2O aerosol on ice nucleation in the upper troposphere using a global chemistry and transport model

Xiaohong Liu and Joyce E. Penner

Department of Atmospheric, Oceanic and Space Sciences, University of Michigan, Ann Arbor, Michigan, USA

Received 9 February 2001; revised 23 October 2001; accepted 12 November 2001; published 20 June 2002.

[1] A 2-year simulation of Mount Pinatubo volcanic aerosol is performed using a global chemistry and transport model. The model is driven by meteorological fields from the NASA Goddard Data Assimilation Office (DAO) general circulation model (GCM) with a horizontal resolution of 2° latitude by 2.5° longitude and 46 vertical levels. The model reproduces the equatorial aerosol reservoir bounded between 20°S and 30°N several months after the eruption and the detrainment of sulfate aerosol from the equatorial reservoir occurring in connection with anticyclonic circulation systems. Our model results are generally consistent with the dispersal characteristics of sulfate aerosol derived from the Stratospheric Aerosol and Gas Experiment II (SAGE II) aerosol extinction observations. On the basis of global distribution of Pinatubo sulfate, the homogeneous ice nucleation rate of H_2SO_4/H_2O aerosol (number of aerosol particles freezing per cm^3 of air mass and per second) in the lower stratospheric and upper tropospheric regions is calculated and compared with those of natural and anthropogenic sulfate from sources injected near Earth's surface. Large ice nucleation rates from Pinatubo H_2SO_4/H_2O aerosol are found in the region near the equatorial tropopause and generally in the regions along the tropopause in the bottom of the main Pinatubo aerosol layer during the first year following the eruption. Ice nucleation rates of Mount Pinatubo H_2SO_4/H_2O aerosols are much larger than those of sulfate aerosols from the surface sources in many regions of the upper troposphere during the first year and could still be comparable to rates from these background sources during the second year after the eruption. Our results suggest that the Pinatubo sulfate aerosol could have influenced cirrus formation and evolution globally through homogeneous ice nucleation, although the exact impact also requires a more complete calculation that includes cirrus cloud dynamics and microphysics. Available satellite observations support the above assertion. *INDEX TERMS:* 0305 Atmospheric Composition and Structure: Aerosols and particles (0345, 4801); 0320 Atmospheric Composition and Structure: Cloud physics and chemistry; 0370 Atmospheric Composition and Structure: Volcanic effects (8409); *KEYWORDS:* volcanic aerosol, H_2SO_4/H_2O aerosol, homogenous ice freezing, cirrus cloud, global modeling

1. Introduction

[2] The eruption of the Mount Pinatubo volcano in the Philippines (15.1°N, 120.4°E) on 14–16 June 1991 produced a significant impact on Earth's radiative processes, atmospheric circulation, and stratospheric chemistry [*McCormick et al.*, 1995; *Young et al.*, 1994]. The eruption injected 14–26 megatons of gaseous SO_2 into the stratosphere reaching as high as 30 km [*Krueger et al.*, 1995; *McCormick et al.*, 1995]. The SO_2 was quickly transformed into H_2SO_4/H_2O aerosol with an *e*-folding time of ~35 days [*Bluth et al.*, 1992; *Read et al.*, 1993]. With an estimated total aerosol mass loading of 30 megatons [*McCormick and Veiga*, 1992] the eruption of Mount Pinatubo caused what is believed to be the largest aerosol perturbation to the stratosphere in the 20th century. The bulk of the volcanic cloud quickly moved westward and circled the globe in ~3 weeks after the eruption [*Bluth et al.*, 1992]. Within 2 weeks a substantial part of the Pinatubo cloud had crossed the equator and extended to ~10°S [*Bluth et al.*, 1992].

[3] In the first 1–2 months after the eruption, the bulk of aerosol cloud was confined to the tropics between 20°S and 30°N [*McCormick and Veiga*, 1992; *Stowe et al.*, 1992] and a tropical stratospheric reservoir of aerosol material was formed [*Trepte et al.*, 1993; *Grant et al.*, 1996]. This tropical reservoir is strongly influenced by the phase of the quasibiennial oscillation (QBO) [*Trepte and Hitchman*, 1992]. The reservoir is stable during the QBO easterly shear, while the aerosol tends to spread toward the poles during westerly shear [*Choi et al.*, 1998]. The Mount Pinatubo volcano erupted during the easterly phase of

0148-0227/02/2001JD000455

QBO, and thus observations have shown a long persistence of the tropical maximum. Two to three months after the eruption some Pinatubo material had spread to southern midlatitudes [*Stowe et al.*, 1992; *Minnis et al.*, 1993]. Below 20 km the Pinatubo material spread relatively quickly northward to middle and high latitudes [*McCormick and Veiga*, 1992; *Osborn et al.*, 1995]. Two regimes for the poleward transport of Mount Pinatubo volcanic aerosol during the first 10 months after the eruption were presented by *Trepte et al.* [1993]: transport into the boreal summer hemisphere in the lower regime just above the tropopause and dispersal into the austral winter hemisphere in the upper transport regime near 30 hPa. The detrainment of aerosol from the equatorial reservoir was mainly connected with synoptic-scale events. One year after the eruption the volcanic aerosol was globally distributed in latitudinally banded structures [*Trepte et al.*, 1994].

[4] Over the course of time, volcanic aerosol was transported from the stratosphere into the troposphere through tropopause folding events and through gravitational sedimentation of the aerosol. In the troposphere, volcanic aerosol was removed by dry and wet deposition to Earth's surface. The global sulfate aerosol mass loading reached a maximum in October 1991 and decayed with an *e*-folding time of $\sim$1 year thereafter [*McCormick et al.*, 1995; *Lambert et al.*, 1997].

[5] Remote and in situ measurements of Pinatubo aerosol have shown that the Pinatubo H_2SO_4/H_2O aerosol had a larger effective radius than does the background aerosol for several years after the eruption [*Deshler et al.*, 1992, 1993; *Russell et al.*, 1996]. The larger sizes and number concentration of the Pinatubo H_2SO_4/H_2O aerosol could have a significant impact on ice nucleation and cirrus cloud microphysics in the upper troposphere [*Jensen and Toon*, 1992; *Sassen*, 1992; *Sassen et al.*, 1995]. Cirrus clouds cover $\sim$20–50% of Earth's surface and play a major role in the global radiation budget [*Ramanathan et al.*, 1983; *Mitchel et al.*, 1988]. Hence even moderate changes in cirrus radiative properties could be important. The radiative properties of cirrus clouds depend on their ice water content, ice crystal size distribution, crystal shapes, number concentrations, and other microphysical properties [e.g., *Liou*, 1986]. Microphysical simulations by *Jensen and Toon* [1992] using a one-dimensional (1-D) microphysical cirrus model that included the homogeneous nucleation of sulfate aerosol suggested that at temperatures below about -50°C the concentrations of ice crystals which nucleate may be as much as a factor of 5 larger when volcanic aerosols >0.2 μm are present. Satellite observations in the Earth Radiation Budget Experiment (ERBE) have shown evidence of an increase in the extinction coefficient of optically thick clouds during the initial posteruption period of the Pinatubo eruption [*Minnis et al.*, 1993]. Also, a significant increase in cirrus cloud cover was observed in 1991 based on the National Oceanic and Atmospheric Administration (NOAA) High-Resolution Infrared Radiation Sounder (HIRS) data [*Wylie et al.*, 1994]. However, the global impact of Pinatubo aerosols on ice nucleation in the upper troposphere has not been determined from a global modeling approach.

[6] In this paper we present calculations of the evolution of the Mount Pinatubo aerosol cloud simulated with the Lawrence Livermore National Laboratory (LLNL) global chemistry and transport model IMPACT. The homogeneous ice nucleation rate in the upper tropospheric and lower stratospheric regions is calculated on the basis of the above spatial distribution of Pinatubo H_2SO_4/H_2O aerosol. The effect of Pinatubo aerosol on the upper level ice nucleation rates is discussed in comparison with sulfate aerosol from Earth's surface sources.

2. Model Description

[7] A global chemistry-transport model, LLNL/IMPACT, was utilized in this study. The IMPACT model is developed as a code capable of using massively parallel computer architectures, and the simulations reported here were run on 32 processors of the Cray T3E. For this study, IMPACT was driven by meteorological fields available at a 6-hour time interval from the NASA Goddard Data Assimilation Office (DAO) general circulation model (GCM) and interpolated to a 1-hour time interval. The spatial resolution of IMPACT is the same as the DAO assimilated meteorological data, which has a horizontal resolution of 2° latitude by 2.5° longitude. The vertical resolution varies with different versions of the DAO Goddard Earth Observing System version 1 (GEOS-1). Because the data for 1991 are only available at low vertical resolution (20 sigma levels with the model top at 10 hPa), we used data from 1997 to 1998 to model the spread of the Pinatubo aerosol. This time period covers approximately the same phase of the QBO as that for the actual Pinatubo eruption. There are 46 sigma levels for the 1997/1998 data with more than half of them in the stratosphere and the model top is at 0.1 hPa (mean pressure levels of 994, 971, 930, 875, 813, 745, 675, 605, 537, 472, 410, 353, 302, 258, 220, 187, 158, 133, 112, 94.1, 79.3, 67.0, 56.7, 48.1, 41.0, 35.0, 29.9, 25.5, 21.8, 18.5, 15.7, 13.1, 10.9, 8.96, 7.28, 5.83, 4.61, 3.58, 2.73, 2.03, 1.47, 1.03, 0.69, 0.44, 0.27, and 0.15 hPa). The vertical resolution is around 1 km in the altitude range between 5 and 20 km. The relatively high vertical resolution in the upper tropospheric and lower stratosphere assures a numerically accurate representation of tracer transport in the lower stratosphere and upper troposphere and makes possible a study of the exchange of trace species between the stratosphere and troposphere.

[8] The IMPACT model uses a flux-form semi-Lagrangian advection scheme [*Lin and Rood*, 1996]. Dry deposition rates are calculated using a package developed at Harvard University based on the work of *Jacob and Wofsy* [1990], *Wesely* [1989], and *Walcek et al.* [1986]. Wet deposition is distinguished between two types of precipitation, convective and large scale. A wet convective scavenging parameterization is employed which is based on the convective mass flux occurring in the GCM convective events [*Balkanski et al.*, 1993]. A given percentage (called the scavenging efficiency) of aerosol and gaseous species is removed from upward moving air for all wet convective events. The *Giorgi and Chameides* [1986] first-order rainout parameterization is used for both large-scale and convective precipitation in addition to scavenging in wet convective updrafts. Washout by large-scale precipitation is computed as a first-order loss process using a washout

rate constant of 0.1 mm^{-1} normalized to the precipitation rate in the precipitating fraction of the grid box [*Balkanski et al.*, 1993]. Cumulus transport in the IMPACT model was derived from the relaxed Arakawa-Schubert scheme, which has been described in detail by *Penner et al.* [1998]. The cumulus mass flux and convective cloud detrainment used in the scheme are derived from the DAO meteorological fields. The LLNL/IMPACT model is described more fully by D. Rotman (D. Rotman et al., IMPACT, the LLNL 3-D global troposphere-stratosphere chemical transport model: A model description, submitted to *Journal of Geophysical Research*, 2001).

[9] For the simulation of Mount Pinatubo clouds, for simplicity, two chemical species were considered, sulfur dioxide (SO_2) and sulfuric acid particles (H_2SO_4). SO_2 is assumed to be quickly converted to H_2SO_4 with an *e*-folding time of 35 days [*Bluth et al.*, 1992; *Read et al.*, 1993]. Similar to the middle atmosphere (MA) European Center/Hamburg version 4 Pinatubo simulation [*Timmreck et al.*, 1999] we assume an initial volcanic cloud mass of 17 Tg SO_2, as observed by the Microwave Limb Sounder and Total Ozone Mapping Spectrometer (TOMS) [*Read et al.*, 1993; *Krueger et al.*, 1995]. The Pinatubo SO_2 is initialized horizontally over the grid boxes between 6°–16°N and 100°–120°E, corresponding to the TOMS observations of 16 June 1991 [*Bluth et al.*, 1992]. Also, the initial SO_2 mass is distributed over eight model layers between 67 and 22 hPa (~19 and 26 km). This distribution corresponds to measurements by aircraft, ship, and lidar, which have shown that the volcanic plume reached up to a height of 30 km, with the bulk of aerosol concentrated between 20 and 27 km in altitude [*McCormick et al.*, 1995]. Gravitational settling is also included for H_2SO_4/H_2O aerosol. A lognormal size distribution with a constant standard deviation of 1.8 is assumed for the Pinatubo sulfate aerosol [*Timmreck et al.*, 1999]. The evolution of the volume mean diameter for the aerosol with the time after eruption is estimated from a variety of measurements of the stratospheric aerosol effective radii (R_{eff}) [*Russell et al.*, 1996]. The slip correction factor for Stokes law and the settling velocity are then calculated [*Seinfeld and Pandis*, 1998]. It should be noted that post-Pinatubo stratospheric aerosol size distributions were usually bimodal [e.g., *Deshler et al.*, 1992; *Pueschel et al.*, 1994a]. In spite of this a unimodal lognormal form was assumed to retrieve size distributions from post-Pinatubo extinction spectra [*Russell et al.*, 1996; *Yue et al.*, 1994], mainly due to the difficulty in constraining retrievals of the six parameters of a bimodal lognormal distribution. A time-dependent correction has been derived from measured biomodal size distributions of *Goodman et al.* [1994] and applied to the retrieved R_{eff} values for the unimodal lognormal size distributions [*Russell et al.*, 1996].

[10] The post-Pinatubo aerosol H_2SO_4/H_2O size distributions derived by *Russell et al.* [1996] were measured in the stratosphere with H_2SO_4 weight percents (the percentages by weight of the H_2SO_4 in the aerosol) of 65–80% for most stratospheric temperatures and humidities. In our study, dry aerosol sizes are estimated assuming an H_2SO_4 weight percent of 75% for *Russell et al.*'s [1996] data. Then the equilibrium radius and composition (molality) of the solution drop for a dry solute particle at a given saturation ratio (S_w) are determined by solving the Köhler equation numerically [*Pruppacher and Klett*, 1997],

$$\ln S_w = \frac{2\sigma_{la}}{R_v T \rho_w r_l} + \ln a_w, \tag{1}$$

where

$$a_w = \exp(-0.001\, \upsilon \Phi_l M_w M). \tag{2}$$

In this expression, σ_{la} is the interfacial surface tension of the solution-air interface, r_l is the solution drop radius, R_v is the ideal gas constant for water vapor, T is the air temperature (K), ρ_w is the density of pure water, a_w is the water activity, υ is the total number of ions into which a salt molecule dissociates, Φ_l is the osmotic coefficient of the solution, M_w is the gram molecular weight of water, and M is the molality,

$$M = \frac{1000\, m_s}{M_s[4\pi r_l^3 \rho_l/3 - m_s]}, \tag{3}$$

where m_s is the dry solute mass, ρ_l is the solution density, and M_s is the gram molecular weight of solute. For solving the Köhler equation, σ_{la} and ρ_l are determined as functions of temperature and molality for pure H_2SO_4/H_2O, as given by *DeMott et al.* [1997]. The above calculated molality of the solution drop is used to estimate the homogeneous freezing rate J_{ls} of an H_2SO_4/H_2O aerosol (per cm^3 of aerosol volume and per second) as shown below. It should be noted that these formulations for σ_{la} and ρ_l are valid for data compiled at $M < 4.2$. For very dry regions with $M > 4.2$ (most of the lower stratosphere) we do not use the Köhler equation to solve the drop equilibrium sizes and composition. Instead, the weight percent of H_2SO_4 in the aerosol (for the bulk aerosol composition) based on the parameterization of *Tabazadeh et al.* [1997] is used to estimate J_{ls}. It does not matter much which method is used because in these dry regions, virtually no ice freezing takes place. Water activity (a_w) versus molality in equation (2) is based on a form suggested by *Chen* [1994], which is given as

$$a_w = 1 \Big/ \left(1 + \sum_i c_i M^i\right). \tag{4}$$

Coefficients c_i are given by *DeMott et al.* [1997]. This semiempirical formulation of a_w was found to agree quite well with the data of *Rard et al.* [1976]. Following *DeMott et al.* [1997], the temperature dependence of water activity was not considered.

[11] The weight percent of H_2SO_4 in the aerosol is determined by the thermodynamics of an H_2SO_4-H_2O drop in equilibrium and is based on the parameterization of *Tabazadeh et al.* [1997]. The H_2SO_4 weight percent is a strong function of temperature and a weaker function of the ambient water vapor partial pressure [*Steele and Hamill*, 1981]. *Tabazadeh et al.* [1997] showed that the *Steele and Hamill* [1981] formulation underestimates the water partial pressure over aqueous H_2SO_4 solution by up to 12% at low

temperatures and derived a new parameterization of H_2SO_4-H_2O aerosol composition based on a thermodynamic model of aqueous sulfuric acid [*Clegg and Brimblecombe*, 1995]. This formulation is valid for relative humidity above 1% in the temperature range of 185–260 K. We use this parameterization to estimate the water percent of H_2SO_4 in the aerosol for the upper troposphere and lower stratosphere. The H_2SO_4 weight percent is used to calculate J_{ls} in regions with $M > 4.2$. It should be noted that this calculated H_2SO_4 weight percent in the aerosol does not explicitly depend on aerosol size.

[12] Solution droplets of a given size and molality are assumed to have an effective freezing temperature [*Sassen and Dodd*, 1988], given by

$$T_{\text{eff}} = T + \lambda \Delta T_m, \tag{5}$$

where ΔT_m is the equilibrium melting point depression (positive valued). For calculating the homogeneous freezing rate J_{ls} of a solution droplet, the effective freezing temperature T_{eff} is used as the solution drop temperature (T) for substituting into the expression for the classical freezing rate for pure water [*DeMott et al.*, 1994, equation (3)]

$$J_{ls0} = 10^y, \tag{6}$$

where $y = -606.3952 - (52.6611T_c) - (1.7439T_c^2) - (0.0265T_c^3) - (1.536 \times 10^{-4}T_c^4)$ and $T_c = T - 273.15$. T_{eff} accounts for the tendency of solution to supercool more strongly than pure water because of the effects of the dissolved materials. This approach has been used in recent studies that estimated the homogeneous freezing rate J_{ls} of sulfate aerosol [*DeMott et al.*, 1994, 1997; *Sassen and Benson*, 2000].

[13] In equation (5), *Sassen and Dodd* [1988] suggested $\lambda = 1.7$ for ammonium sulfate. For sulfuric acid, *DeMott et al.* [1997] assumed $\lambda = 1.0$ on the basis of the measurements of *Bertram et al.* [1996]. In contrast to the flow tube results of *Bertram et al.* [1996], *Koop et al.* [1998] found that the degree of supercooling increased to a greater degree as the weight percent of H_2SO_4 in droplets increased ($\lambda = 1.9$) using an optical microscope technique. More recent experiments by *Chen et al.* [2000] using a continuous flow thermal diffusion chamber suggested $\lambda = 1.75$ for ammonium sulfate and $\lambda = 1.98$ for sulfuric acid. In the present study we assume that the coefficient for λ is 2.0 for sulfuric acid and also examine the impact of using $\lambda = 1.0$ on our results. The value of ΔT_m in equation (5) for sulfuric acid is determined proportional to the molality of the solution drop on the basis of the parameterization of *DeMott et al.* [1997]. This expression for ΔT_m accurately represents tabulated data for H_2SO_4 weight percent from 0 to ~35% (molality <5.5). This covers most of the range relevant to the upper troposphere. A concentrated droplet with a molality of 5.0 will produce an equilibrium melting point depression as high as ~50°C based on *DeMott et al.*'s [1997] formulation. Thus ice freezing is not possible for concentrated droplets with molality >5.5, and *DeMott et al.*'s [1997] formulation for ΔT_m is adequate. Once the J_{ls} of a given droplet or haze size is estimated, the total concentration of solution droplets or haze particles freezing in some increment of time Δt may be given as

$$N_f = \int_0^\infty (1 - \exp(-J_{ls}V_l\Delta t))n(r_l)dr_l, \tag{7}$$

where V_l ($V_l = 4\pi r_l^3/3$) is the volume of solution droplets (cm^3) with radius r_l calculated from the Köhler equation, $n(r_l)dr_l$, and is the droplet number (cm^{-3}) between r_l and $r_l + dr_l$. $N_f/\Delta t$ can be thus regarded as the homogeneous ice nucleation rate J_n of droplets or haze particles (per cm^3 of air mass and per second) averaged over the time period Δt. We use $\Delta t = 1$ s in this study, which is short compared with the interval of meteorological data (e.g., temperature and relative humidity with respect to water (RH_w)) in the model. Since we are interested in the contrast between the Pinatubo and surface aerosol ice nucleation rates, which are evaluated under the same Δt, this time interval is sufficient.

[14] The homogeneous ice nucleation rate of sulfate aerosol from surface sources (both anthropogenic and natural) in the upper troposphere and lower stratosphere are also calculated in order to compare with that of Pinatubo sulfate. Because model results for a detailed tropospheric sulfur cycle using IMPACT are currently not available, the spatial distribution of sulfate mass mixing ratio from surface sources was simulated with the global chemistry/climate model GRANTOUR/Community Climate Model, version 1 (CCM1) [*Penner et al.*, 1991, 1994]. The simulated sulfate is in reasonable agreement with observations [e.g., *Penner et al.*, 1994; *Chuang et al.*, 2002] and with other chemical transport models [*Penner et al.*, 2001]. GRANTOUR/CCM1 uses a highly accurate Lagrangian tracer transport scheme, but the basic meteorology driving the model uses a sigma coordinate system with 12 vertical levels (mean pressure levels of 991, 926, 811, 664, 500, 355, 245, 165, 110, 60, 25, and 9 hPa) and a horizontal resolution of ~4.5° × 7.5°. The simulated sulfate distributions are thus interpolated to the IMPACT grid. The anthropogenic sulfate includes sulfur from fossil fuels and industry (~76 Tg S yr^{-1}) and biomass burning (~2.2 Tg S yr^{-1}). The natural sulfur includes dimethyl sulfide emissions from the oceans (~24 Tg S yr^{-1}) as well as SO_2 emissions from volcanoes (~9 Tg S yr^{-1}).

[15] The aerosol composition can have important implications for ice nucleation. Unfortunately, very little is known about the chemical composition of upper tropospheric aerosols and the degree of ammoniation of the sulfate compound from surface sources. Therefore ice nucleation rates for both sulfuric acid and ammonium sulfate are calculated for sulfate aerosol from surface sources. The same initial dry size distribution is assumed for sulfuric acid and ammonium sulfate. The size distribution is taken from measurements made during the Global Backscatter Experiment (GLOBE) [*Pueschel et al.*, 1994b]. A lognormal distribution ($r_0 = 0.02$ μm, $\sigma = 2.3$) was fit to represent the measured distribution [*Jensen et al.*, 1994; *Jensen and Toon*, 1994], which appears to be typical of the upper tropospheric aerosol [*Pueschel et al.*, 1994b]. In our study this distribution is used for both natural and anthropogenic sulfate in the upper troposphere. For ammonium

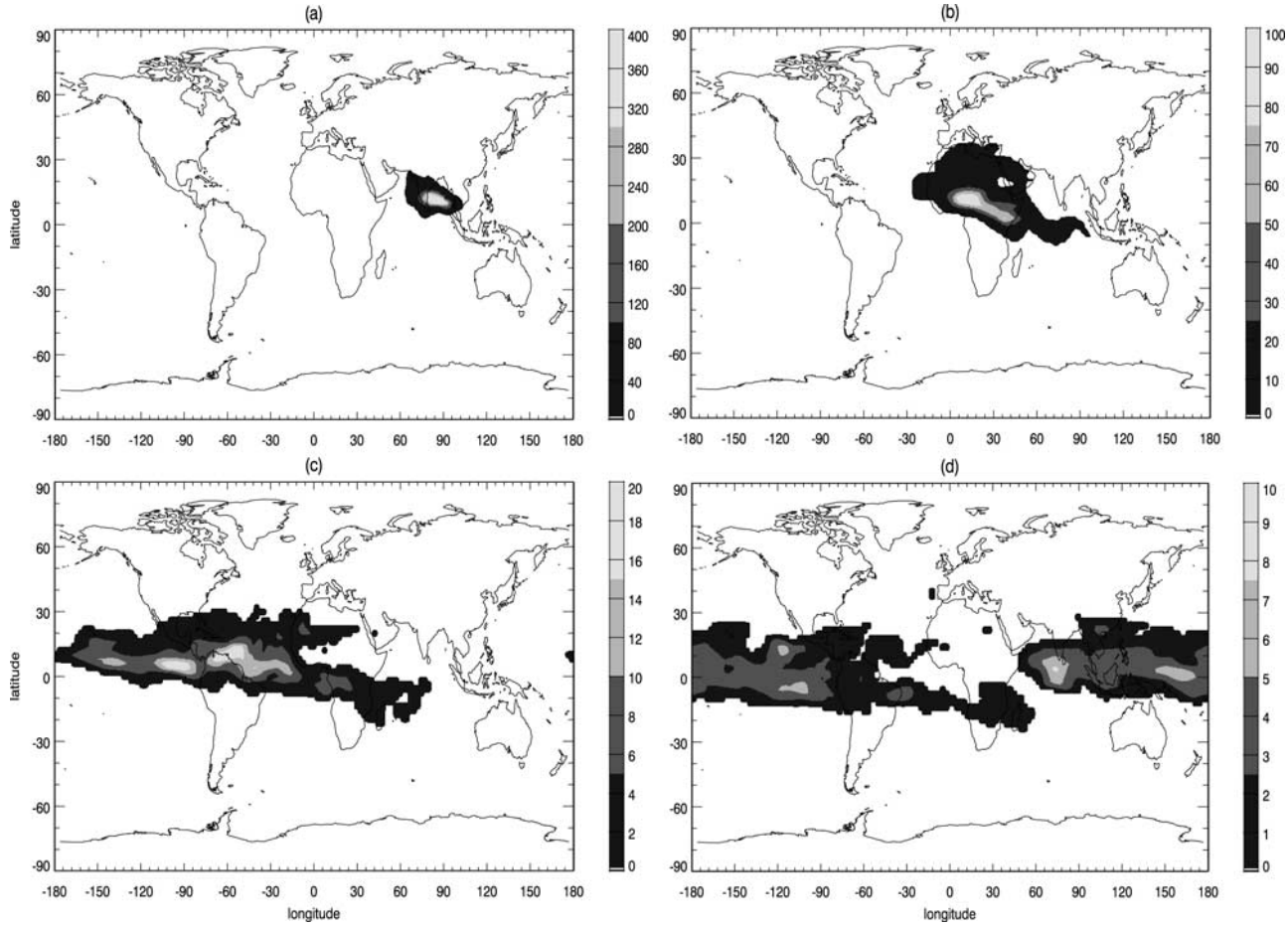

Figure 1. Initial dispersal of the total SO_2 column amount for (a) 18 June 1991, (b) 23 June 1991, (c) 30 June 1991, and (d) 7 July 1991. Total column amounts of SO_2 are given in units of milliatmosphere centimeters in order to compare with the Total Ozone Mapping Spectrometer (TOMS) measurements [*Bluth et al.*, 1992]. This unit is given in terms of the 1-D thickness of the pure gas layer at standard temperature and pressure.

sulfate the interfacial surface tension of the solution-air interface σ_{la}, solution density ρ_l as a function of temperature, and solution molality were as given by *DeMott et al.* [1994], and the water activity a_w and equilibrium melting point depression ΔT_m as a function of solution molality were given by *Fitzgerald* [1974] and *DeMott et al.* [1997], respectively. The coefficient for λ is assumed to be 1.7. Ammonium sulfate will not deliquesce until RH_w exceeds ~82% [*Pruppacher and Klett*, 1997]. Thus we assume that homogeneous freezing of $(NH_4)_2SO_4$ aerosol will not occur if the $RH_w < 82\%$ [*Heymsfield and Sabin*, 1989].

3. Results and Discussion

3.1. Modeling of Mount Pinatubo Cloud

[16] Figure 1 shows the initial dispersal of the total SO_2 column amount. The SO_2 cloud moved rapidly westward after the eruption in accordance with the TOMS observations [*Bluth et al.*, 1992]. By 18 June the main portion of the SO_2 cloud is centered over the Bay of Bengal. By 23 June, 1 week after the eruption, the SO_2 cloud is located over central Africa. By 30 June, 2 weeks after the eruption, the cloud has spread from the east Pacific Ocean to the west coast of Africa, with the leading edges located in the central Pacific Ocean. The SO_2 cloud circled the globe in ~20 days (see Figure 1d), and the cloud had crossed the equator to as far as 10°S. Later on the SO_2 cloud was below the TOMS detection limit due to the chemical conversion to H_2SO_4 aerosol particles [*Bluth et al.*, 1992].

[17] A notable feature for the Pinatubo H_2SO_4 aerosol from the satellite observations is the tropical stratospheric reservoir [*Trepte and Hitchman*, 1992; *McCormick and Veiga*, 1992; *Hitchman et al.*, 1994]. Possible reasons for this reservoir are subtropical quasipermeable barriers with strong potential vorticity (PV) gradients, which inhibit transport of tropical air into the subtropics [*Trepte and Hitchman*, 1992]. Analyses of SAGE II 1-μm stratospheric aerosol extinction ratio data by *Trepte et al.* [1993] showed that in the Northern Hemispheric winter of 1991/1992, two distinct transport regimes existed in the lower tropical stratosphere: a lower transport regime just above the tropopause with rapid poleward movements and an upper transport regime near 30 hPa associated with planetary wave activity in the southern subtropics. In the upper transport regime, rapid detrainment of aerosols from the upper tropical reservoir also depends on the phase of QBO [*Trepte*

and Hitchman, 1992]. Mount Pinatubo erupted during the easterly phase of the QBO, planetary waves were shielded from the equator, and only aerosol lying near the subtropics experienced further poleward mixing.

[18] In order to compare our results directly with the SAGE II observations presented by *Trepte et al.* [1993], the aerosol extinction ratio at a wavelength of 1 μm was calculated. The aerosol extinction ratio is defined as the total extinction observed at a wavelength of 1 μm normalized by Rayleigh extinction and is analogous to the species mixing ratio [*Russell et al.*, 1981]. The Mie scattering coefficient was computed on the basis of our simulated H_2SO_4 mass mixing ratio and the aerosol size distributions given by *Russell et al.* [1996]. The temperature and pressure from the DAO meteorological data were used. Figure 2 shows the zonal mean 1-μm extinction ratio calculated in this study for a period of 10 months after the eruption (from 15 July 1991 to 15 April 1992). We see in Figure 2a that there was a reservoir of volcanic material throughout the tropics, primarily bounded between 30°S and 20°N, which extended from the tropopause to a height of 27 km. During the month following the eruption some aerosol had transported to middle and high northern latitudes below ~18 km. In the upper levels between 20 and 25 km, poleward transport took place in the Southern Hemisphere. This transport of material into the Southern Hemisphere was linked with the transient penetration of the polar vortex into the tropics. In the lower transport regime the movement of aerosol into northern midlatitudes was associated primarily with monsoonal circulation [*McCormick and Veiga*, 1992; *Trepte et al.*, 1993]. Two months (Figure 2b) and three months (Figure 2c) after the eruption, in the Southern Hemisphere, an enhanced layer of extinction ratio several kilometers thick protruded from the tropical aerosol reservoir centered near ~21 km. The southern midlatitudes showed a dramatic increase in aerosol loading below 30 km. A sharp extinction ratio gradient was established between 60° and 70°S, extending from the tropopause to ~30 km, which shows the isolation of air inside the polar vortex from the changing aerosol environment outside the vortex [*McCormick et al.*, 1983; *Juckes and McIntyre*, 1987]. The Mount Pinatubo aerosol dispersed further north beyond 30°N in Figures 2b and 2c, yet aerosol conditions remained unperturbed north of 60°N above 25 km. Therefore the shapes and boundaries of our simulated Pinatubo aerosol cloud for the first 3 months after the eruption are quite similar to those of *Trepte et al.* [1993]. These transport patterns are also supported by other observations [*Stowe et al.*, 1992; *Minnis et al.*, 1993].

[19] Figures 2c, 2d, and 2e show the continued propagation of the Mount Pinatubo aerosol into the Southern Hemisphere. At the same time, northward transport of the Pinatubo aerosol during the boreal autumn is also evident. This correlates with significant wave activities which transported aerosol to middle and high latitudes [*Trepte et al.*, 1993]. While the shapes and boundaries of our simulated Pinatubo cloud are consistent with those of *Trepte et al.* [1993], the densest portion of the Pinatubo aerosol layer (circled in yellow in Figure 2) in the Southern Hemisphere south of 30°S has penetrated into the troposphere faster than the observations from October 1991. Thus downward transport of our simulated Pinatubo aerosol into the troposphere might be too fast in this region. One possible reason for this might be that the settling velocity used in this region was larger than that for the actual Pinatubo aerosol. The effective radius of Pinatubo aerosol presented by *Russell et al.* [1996] with time was used in our study, but the spatial variation of the Pinatubo aerosol sizes was not considered since no information was available. There may be two other important reasons for the downward transport. One is that these DAO meteorological fields have excessive cross-tropopause flux by up to a factor of ~2 (P. Connell, personal communication, 2001). The second is that this version of the LLNL/IMPACT model was not corrected for the inconsistency between the surface pressure tendency and the divergence of the winds in our meteorological fields. This inconsistency leads to nonconservation of tracer mass. We examined this nonconservation of mass and found it to be of order 25% after a 1.5-year simulation. This is sufficiently small that it does not affect our main conclusions, but the details of the transport are affected. We also found that northward transport of our simulated Pinatubo cloud after December 1991 is not as strong as that presented by *Trepte et al.* [1993]. The impact of these differences on our estimated ice freezing will be discussed in section 3.2. Similar to the observations presented by *Trepte et al.* [1993], the aerosol cloud over the tropics kept rising, and the top reached an altitude of ~40 km by the middle of November (Figure 2e). The cloud top stayed near the 40 km altitude through February 1992. This feature is produced by the vertical transport of aerosol particles by the Brewer-Dobson meridional circulation, which took place in the easterly shear of the semiannual oscillation (SAO) near 35 km and the QBO in the lower stratosphere [*Trepte and Hitchman*, 1992; *Trepte et al.*, 1993]. Later on the Pinatubo cloud retained the overall meridional structure evident in December 1991 (Figures 2f, 2g, and 2h). The Pinatubo cloud over the tropics and Southern Hemisphere, however, descended due to gravitational settlement or transport over the equator caused by the descending westerlies of the SAO during March and April [*Trepte et al.*, 1993], while that over the northern extratropics continued to rise until April 1992, at which time rapid descent started.

[20] Our results reproduce many of the zonal mean dispersal characteristics of Pinatubo aerosol cloud as described by *Trepte et al.* [1993] based on the SAGE II observations. Our simulation results are also generally consistent with the dispersal features of the Pinatubo aerosol based on the global latitude-longitude maps of monthly mean aerosol extinctions derived from the SAGE II data [*Rind and Liao*, 1997]. As an example, Figure 3 shows the sulfate mass mixing ratio at 30 hPa (~24 km) on (1) 15 August 1991, (2) 15 September 1991, and (3) 15 October 1991. From Figure 3 the Pinatubo aerosol cloud was mainly constrained between 20°S and 30°N in the 2–4 months after the eruption. However, the aerosol mass continued to transport poleward. There was a strong gradient in the region 60–70°S separating the polar vortex air from the air influenced by the Pinatubo aerosol, which is also evident in the latitude-altitude cross sections of the Pinatubo extinction ratio in Figure 2. A notable feature in Figure 3 is how the sulfate mass was drawn poleward from the equatorial reservoir. Several tongues of a high sulfate mixing ratio can be found, such as the one near Australia

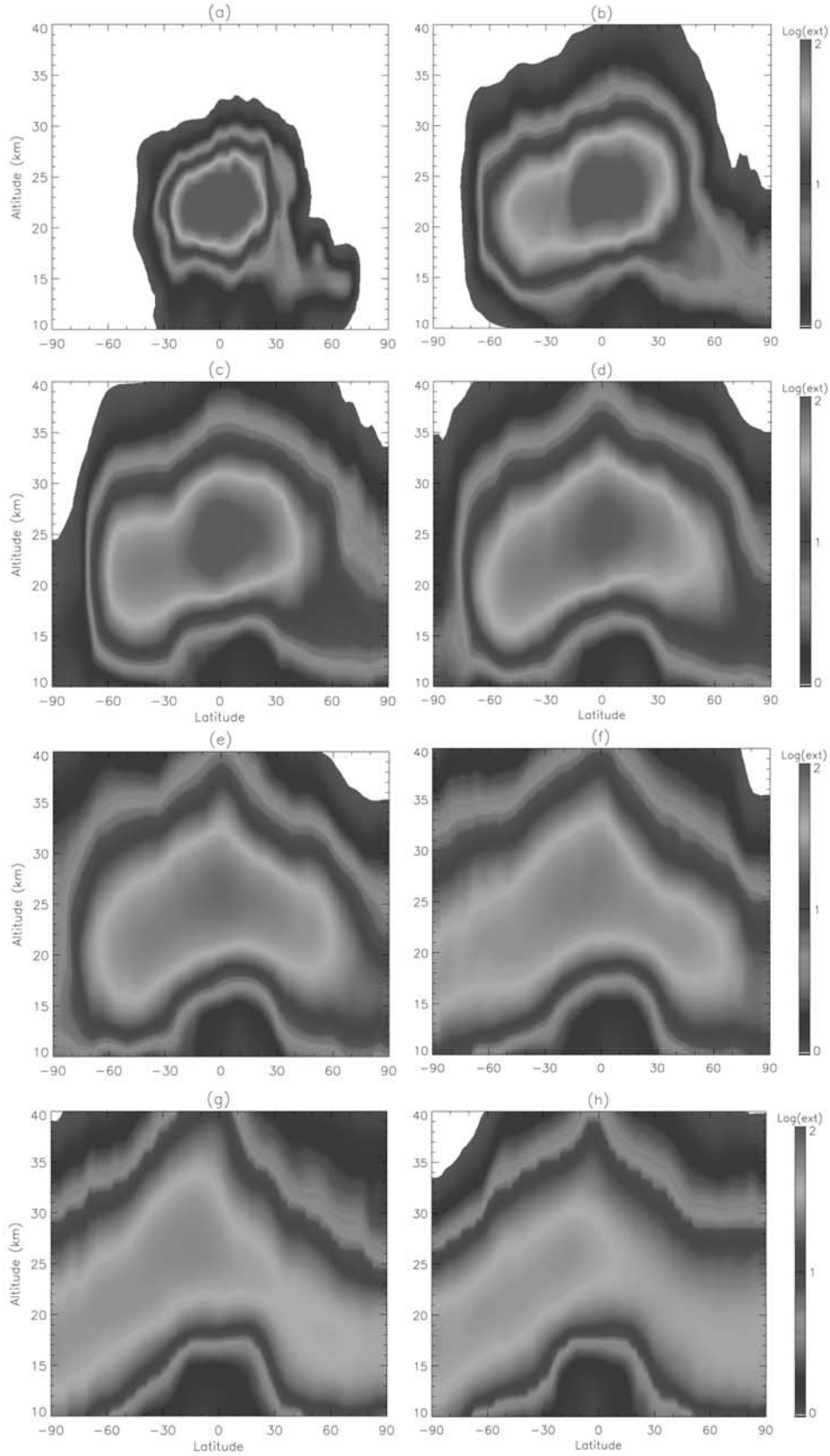

Figure 2. Latitude-altitude cross sections of the extinction ratio for (a) 15 July 1991, (b) 15 August 1991, (c) 15 September 1991, (d) 15 October 1991, (e) 15 November 1991, (f) 15 December 1991, (g) 15 February 1992, and (h) 15 April 1992. A logarithmic scale is used for the extinction ratio. See color version of this figure at back of this issue.

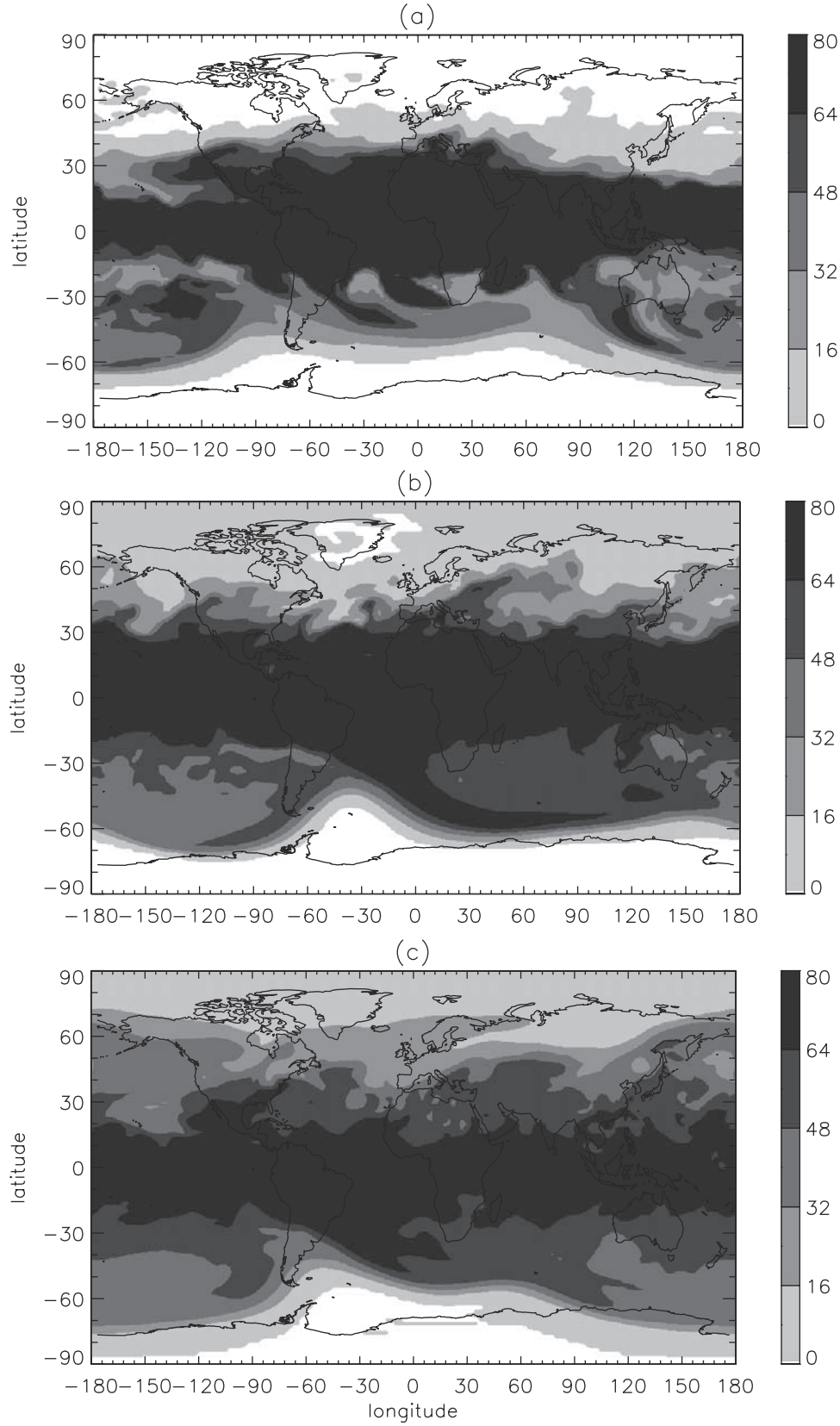

Figure 3. Sulfate mass mixing ratio (ppbm) at 30 hPa for (a) 15 August 1991, (b) 15 September 1991, and (c) 15 October 1991.

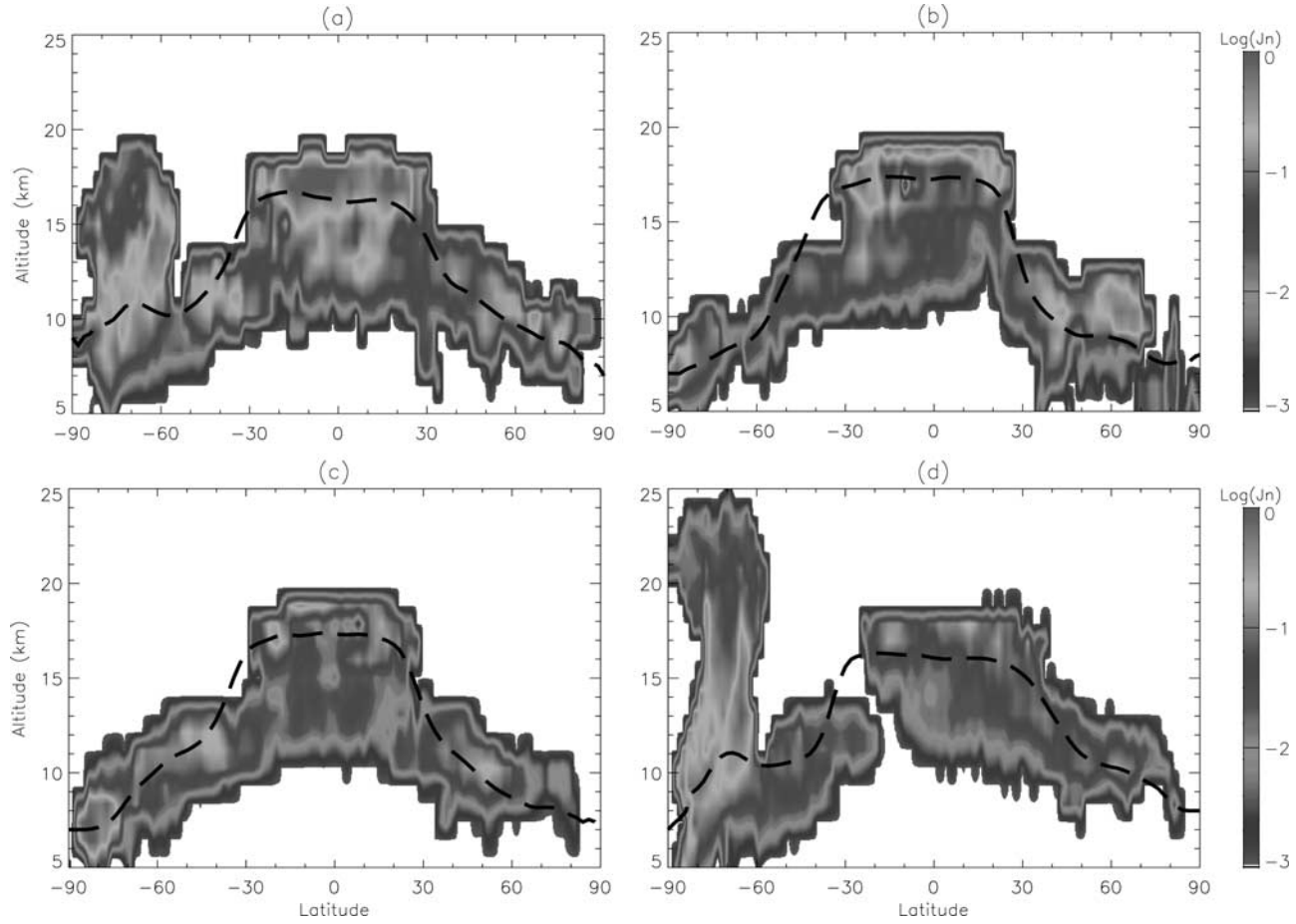

Figure 4. Latitude-altitude cross sections of the homogeneous ice nucleation rate J_n (cm^{-3} s^{-1}) of Mount Pinatubo H_2SO_4/H_2O particles as a function of post-Pinatubo time for (a) 15 October 1991, (b) 15 January 1992, (c) 15 April 1992, and (d) 15 July 1992. A logarithmic scale is used for the nucleation rates. The dashed line shows the model calculated tropopause. See color version of this figure at back of this issue.

(Figure 3a) and two extending from the coast of Brazil to the south Indian Ocean (Figures 3b and 3c). These transport characteristics were associated with transient planetary wave activity when intense anticyclonic circulation systems formed [*Trepte et al.*, 1993; *Osborn et al.*, 1995]. Higher aerosol extinction can also be found in regions in connection with these tongues in the SAGE II data during the same time period [*Rind and Liao*, 1997].

3.2. Ice Nucleation Rates of Sulfate: Mount Pinatubo Versus Surface Sources

[21] The homogeneous ice nucleation rate of H_2SO_4/H_2O particles in the lower stratosphere and upper troposphere was calculated on the basis of the simulated distributions of the Mount Pinatubo sulfuric acid mass mixing ratio. In this section, zonally averaged nucleation rates are shown. High zonally averaged nucleation rates indicate that strong nucleation events could take place and thus are linked to the frequency of cirrus occurrence, although the high ice nucleation rate regions do not necessarily represent high-level cloud coverage. The latter also depends on atmospheric dynamics. Figure 4 shows the zonal mean distributions of the nucleation rate of Mount Pinatubo H_2SO_4/H_2O particles as a function of post-Pinatubo time. The dashed line in this and in subsequent figures shows the model calculated tropopause. Figures 5, 6, and 7 show the zonal mean distributions of corresponding air temperature, RH_w, and H_2SO_4 weight percent in aerosol, respectively. Figure 4a is for 15 October 1991, 4 months after the eruption when the global Pinatubo H_2SO_4 burden is around its maximum due to the conversion of SO_2. The aerosol number concentrations at that time are calculated to be on the order of 10^1-10^2 per cm^3 in the bulk of Pinatubo cloud, which is in the range obtained by the balloonborne measurements [*Deshler et al.*, 1992, 1993]. From Figure 4a, there was a strong maximum region of nucleation rate ($\sim$1.0 cm^{-3} s^{-1}) near the tropical tropopause (16–18 km altitude), which was located at the bottom of Pinatubo cloud layer (see Figure 2). The zonal mean temperature there was lower than −75°C, RH_w was >80%, and H_2SO_4 weight percent was <30% (see Figures 5a, 6a, and 7a). It should be noted that the values given here are zonally averaged. A grid by grid check of RH_w distributions showed that there were many locations around the tropical tropopause with $RH_w > 90\%$. The higher number concentration and relatively larger sizes of Pinatubo H_2SO_4 aerosols (compared with the background aerosols

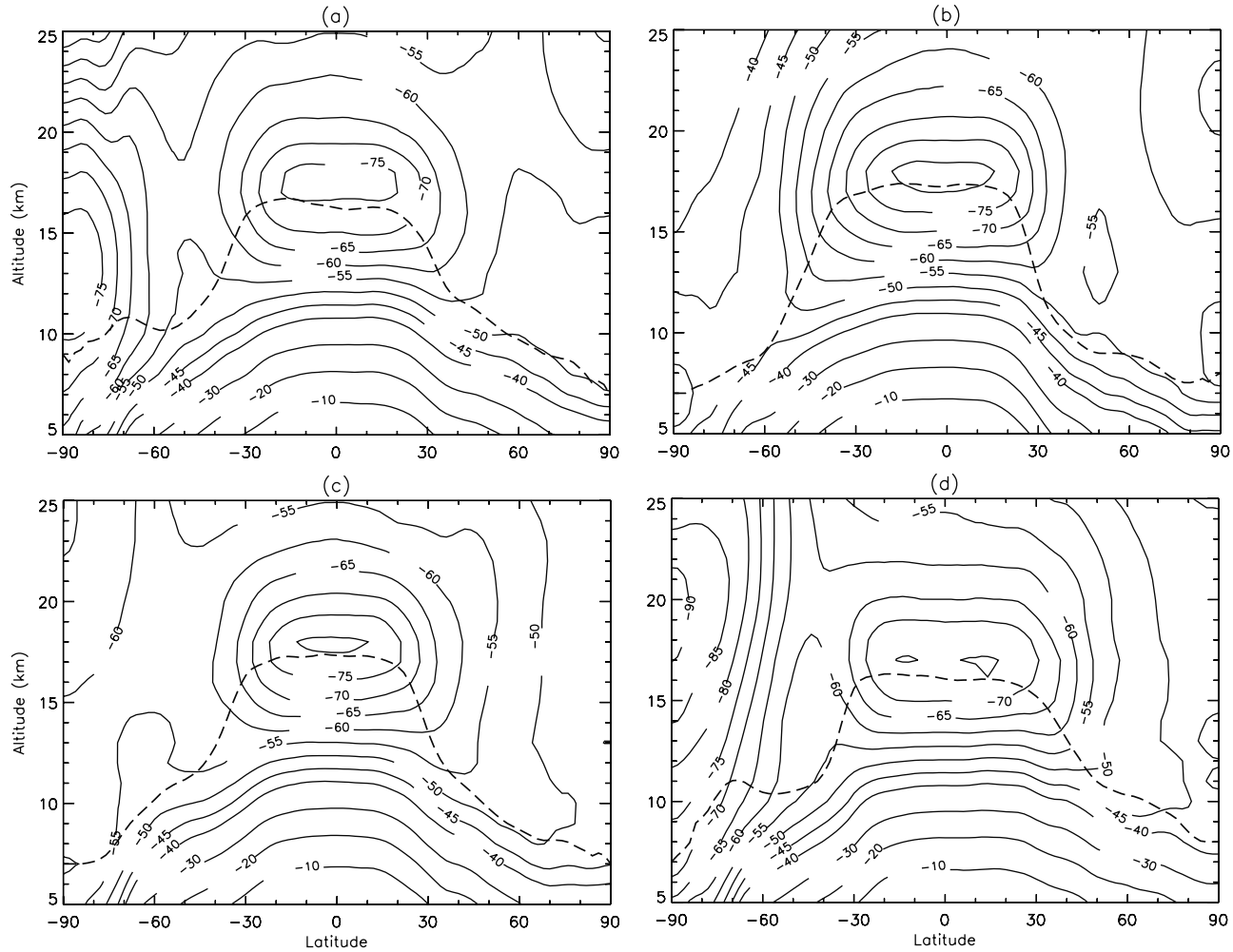

Figure 5. Latitude-altitude cross sections of air temperature (°C). The time period associated with each panel is the same as in Figure 4.

from surface sources) together with high RH_w and low temperature makes the homogeneous freezing of Pinatubo H_2SO_4/H_2O particles in this region very effective. From Figure 4a, there are also large nucleation rates along the tropopause from the tropics to the polar regions located in the lowest portion of the Pinatubo cloud layer. In the Southern Hemisphere near 60°–90°S, there appears to be a region with strong ice-freezing ranging from 7 to 18 km altitude with a maximum from 60° to 70°S and from 12 to ~16 km. The broad maximum in this region closely resembles the distributions of RH_w, which are increasing toward the pole (see Figure 6a). The lower temperatures in the polar region (Figure 5a) in the Southern Hemisphere should also contribute to this region of large ice nucleation rates. Pinatubo sulfate concentrations are decreasing toward the pole, but the combination of low temperature together with relatively high RH_w produces the maximum near 60°–70°S. *Jensen et al.* [1991] calculated the ice nucleation rate of sulfuric acid solution aerosols under stratospheric conditions and found that the nucleation rate is a strong function of temperature for weight percents less than ~20%. We note that in addition to air temperature, RH_w is also a very important factor for ice freezing. Larger RH_w could lower the H_2SO_4 weight percent in aerosol and thus the equilibrium melting point depression ΔT_m. Larger RH_w also increases the aerosol droplet size through the Köhler equation.

[22] Figure 4b is for 15 January 1992, 7 months after the eruption. Strong ice nucleation rates are still present near the tropical tropopause. There were two other regions with large nucleation rates (0.1–1 cm^{-3} s^{-1}): the northern midlatitudes (9–12 km altitude) and the Antarctic region (6–8 km altitude). Both are due to the lower temperature and higher RH_w in the Antarctic (see Figures 5b and 6b). Figure 4c is for 15 April 1992, 10 months after the eruption. The H_2SO_4 global burden and mass mixing ratio were gradually reduced. The aerosol number during this time was in the range of 1–10 cm^{-3} in the Pinatubo cloud layer, which is consistent with the measurements near 19 km altitude (in the Pinatubo cloud layer) over western North America [*Goodman et al.*, 1994]. The ice nucleation rates of H_2SO_4 particles were significantly reduced near the tropical tropopause and in the midlatitude regions. However, the nucleation rate maximum in the Antarctic region increased compared with that shown in Figure 4b. The zonal mean temperature in this region was now

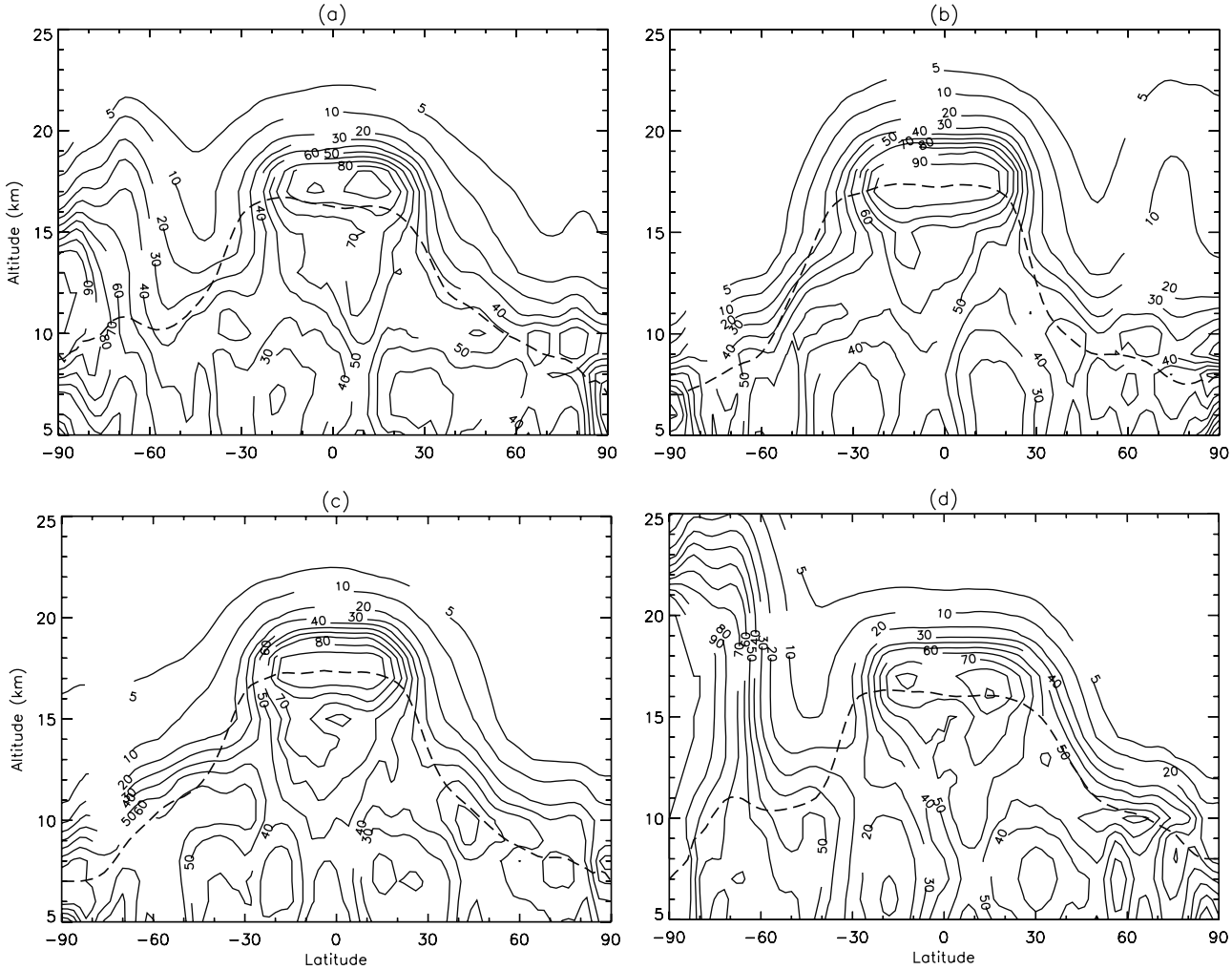

Figure 6. Latitude-altitude cross sections of RH_w (%). The time period associated with each panel is the same as in Figure 4.

reduced from −50°C on 15 January 1992 to less than −55°C on 15 April 1992 (see Figures 5b and 5c). Figure 4d is for 15 July 1992, 13 months after eruption. Ice nucleation rates of H_2SO_4 particles continue to decrease near the tropical tropopause and at midlatitudes, but a region with higher nucleation rates (0.1–1 cm^{-3} s^{-1}) appears in the southern extratropics at altitudes from 5 to 20 km within the Pinatubo cloud layer. The zonal mean temperature and RH_w in this region at this time (austral winter) were below −70°C and were >70%, respectively (see Figures 5d and 6d), which resulted in the high nucleation rates in this region. The freezing of the Pinatubo H_2SO_4 aerosol in the Antarctic region could lead to the formation of polar stratospheric cloud (PSC) particles [*Larson*, 1994] and thus provide a large surface area for heterogeneous chemical reactions in PSCs, which enhance ozone loss in the austral winter and early spring. Record low column ozone in the Antarctic in 1992 and 1993 (e.g., 105 Dobson units on 11 October 1992) and also the near-zero ozone levels in the 14–18 km range in mid-October in these years have been observed [*Hofmann and Oltmans*, 1993; *Hofmann et al.*, 1994].

[23] Figure 8 shows the ice nucleation rate of H_2SO_4/H_2O aerosol solution from natural and anthropogenic surface sources in order to illustrate the impact of Pinatubo H_2SO_4 on background ice nucleation in the upper tropospheric and lower stratospheric regions. Figure 8a, for October, shows that there is a maximum region of ice nucleation rates (0.1–1 cm^{-3} s^{-1}) between the equator and 30°N at the altitudes of 11–13 km, several kilometers lower than the maximum calculated for the Pinatubo aerosols near the tropical tropopause. The lowered maximum is due to the higher number concentration at lower altitudes for H_2SO_4 aerosols from surface sources. This maximum is also correlated with high RH_w. Comparing Figures 4a and 8a, the zonal averaged nucleation rates of Pinatubo H_2SO_4 aerosols were much higher than those of surface H_2SO_4 aerosols in October 1991 in many regions, especially in the Southern Hemisphere. Figure 8b is for January. Comparing with Figure 4b, the zonal mean nucleation rates of Pinatubo H_2SO_4 aerosols were still higher than those of the surface H_2SO_4 aerosols in the northern midlatitudes (30°–70°N) at altitudes of 8–12 km. *Sassen* [1992] and *Sassen et al.* [1995] provided evidence that Pinatubo aerosols signifi-

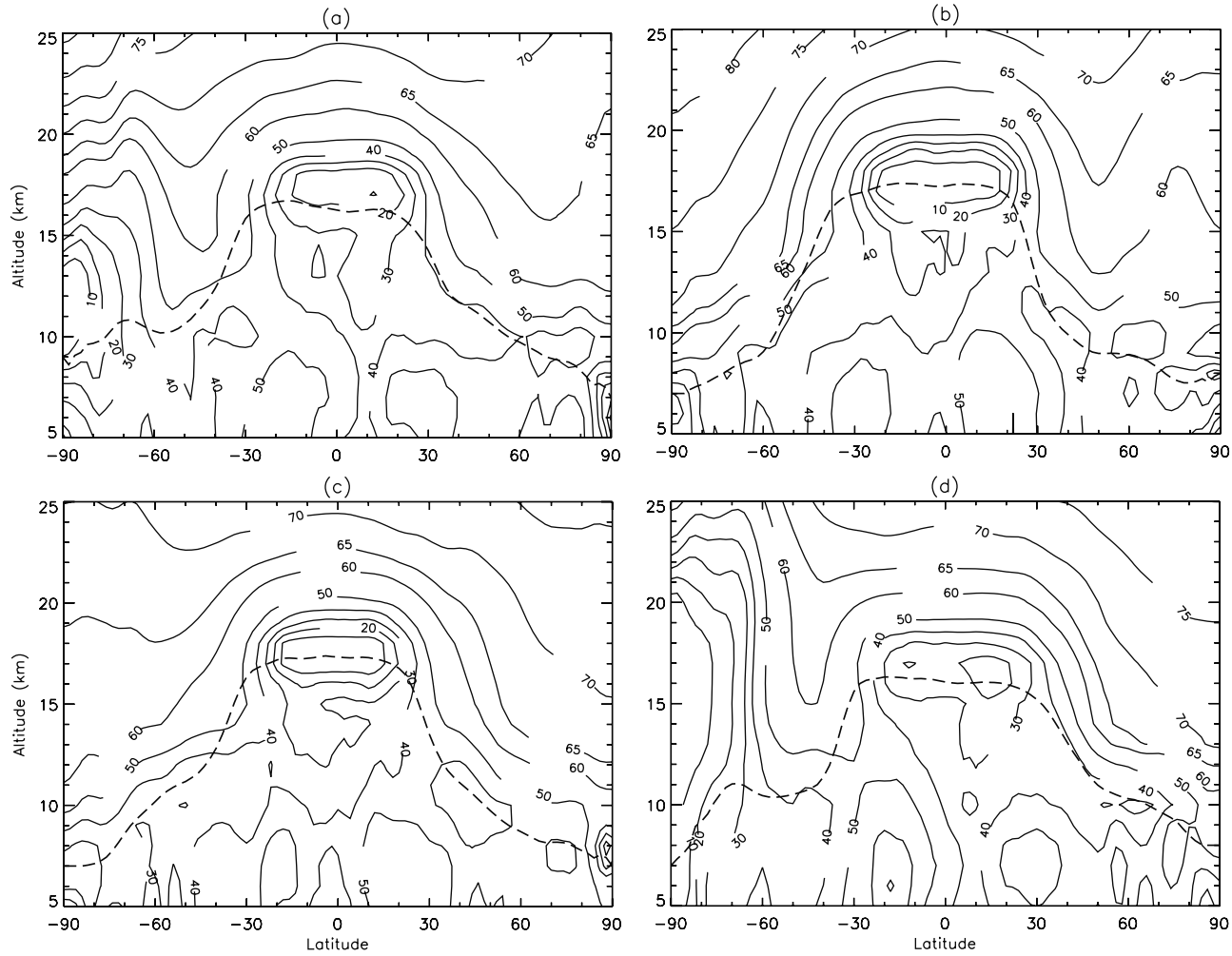

Figure 7. Latitude-altitude cross sections of H_2SO_4 weight percent in aerosol. The time period associated with each panel is the same as in Figure 4.

cantly influenced the formation and maintenance of the cirrus during early December 1991 at Coffeyville, Kansas (37.1°N, 95.6°W). The cirrus clouds being studied were at an altitude of 8–13 km over a temperature range of about −40° to −50 °C. Multiwavelength lidar measurements carried out in Finland (66°N) during the December 1991 to March 1992 European Arctic Stratospheric Ozone Experiment (EASOE) campaign showed high cirrus clouds growing at the base or within the Pinatubo aerosol layer [*Guasta et al.*, 1994]. Figure 8c is for April. Comparing with Figure 4c, the ice nucleation rates of surface H_2SO_4 aerosols are now comparable to those of Pinatubo H_2SO_4 aerosols in magnitude, except in the Antarctic region where the Pinatubo H_2SO_4 aerosol number concentration was much higher due to poleward transport of the aerosol cloud. Figure 8d is for July. There appear regions of high nucleation rates of surface H_2SO_4 aerosols (from equator to 60°N) at altitudes of 10–13 km, mainly due to the large anthropogenic contribution in the Northern Hemisphere. The ice nucleation rates of surface H_2SO_4 aerosols in this region are now overwhelming those of Pinatubo H_2SO_4 aerosols in July 1992. A comparison between Figures 8b and 8d shows that except for the region poleward of 60°S, ice nucleation rates are generally larger in the summer hemisphere than in the winter hemisphere. Satellite HIRS data also indicated more cirrus in the summer than in the winter in each hemisphere [*Wylie et al.*, 1994].

[24] Figures 9a and 9b show the zonal mean nucleation rate of Pinatubo H_2SO_4 aerosols of 15 October 1992 and 15 January 1993, respectively. In Figure 9a the region with strong ice nucleation of Pinatubo H_2SO_4 aerosols between 60°S and the South Pole continues. Comparing with Figures 4a and 4b, 1 year earlier, the zonal mean nucleation rates are now much lower simply due to the decreases of H_2SO_4 mixing ratio and thus the aerosol number concentrations. However, they were still comparable with those of surface H_2SO_4 aerosols in most of the regions.

[25] The results presented above depend upon the ice freezing parameterization. There is still some controversy about the values of the key parameters involved in the equilibrium melting point depression. Apparently, more experiments on homogeneous ice freezing under atmospheric conditions (upper troposphere and lower stratosphere) are needed to address these problems. Thus our estimated absolute values of ice nucleation rates of H_2SO_4 aerosols are preliminary. However, the contrast between

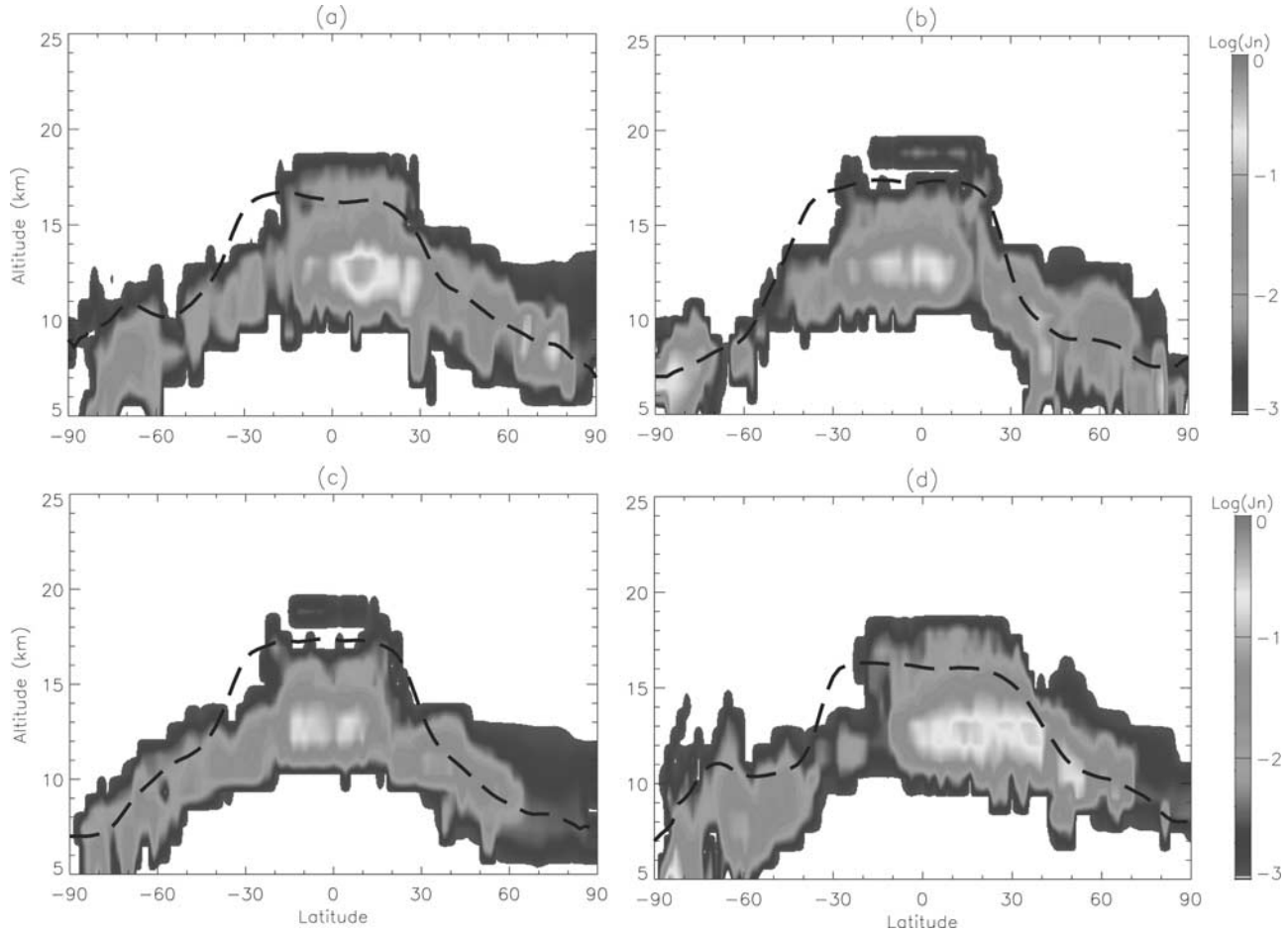

Figure 8. Latitude-altitude cross sections of the homogeneous ice nucleation rate J_n (cm^{-3} s^{-1}) of H_2SO_4/H_2O particles from surface sources (anthropogenic plus natural) in the upper troposphere and lower stratosphere in (a) October, (b) January, (c) April, and (d) July. A logarithmic scale is used for the nucleation rates. See color version of this figure at back of this issue.

Pinatubo and surface H_2SO_4 aerosol nucleation rates and the importance of Pinatubo aerosols to ice freezing in the upper troposphere should be reliable. In the following, some sensitivity tests are discussed in relation to the ice nucleation parameterization. The coefficient for λ in equation (5) reflects the degree of supercooling required for ice formation exceeding the depression of the melting curve. The larger the coefficient for λ, the higher the ice supersaturation is required for the onset of ice formation. In our standard calculations of ice nucleation rates for H_2SO_4 aerosol, $\lambda = 2.0$ is used. The nucleation rates of Pinatubo H_2SO_4 aerosols are calculated again in one sensitivity test using $\lambda = 1.0$ (other parameters were kept the same). Our results show that a decrease in λ from 2.0 to 1.0 results in general increases in the zonal mean nucleation rates (by a factor of <2), while the distribution patterns stay nearly the same. When λ is halved, the nucleation rates in the most humid grid boxes (those with high RH_w) do not change much because of very high J_{ls} for the most diluted aerosol droplets. The equilibrium melting point depression ΔT_m is already quite small for these diluted droplets due to their very low molality. Therefore a change in λ by 1/2 will not obviously influence the effective freezing temperature T_{eff} in equation (5) for these droplets. However, a large change of J_{ls} might take place in those less humid (but not too dry) grid boxes and result in some change of the homogeneous ice nucleation rate J_n (perhaps from 10^{-12} to 10^{-6} cm^{-3} s^{-1}, which is small compared with that in the most humid grid boxes). As a result, the zonal mean nucleation rates are not affected much, but these changes are significant and could introduce a change from clear to cloudy conditions. Therefore a calculation of cloud changes (which requires a dynamical cloud calculation within the atmospheric model in addition to the calculations presented here) may be sensitive to the precise value of λ used.

[26] In section 3.1 we discussed the fact that downward transport of our simulated Pinatubo aerosol cloud might be too fast in the Southern Hemisphere south of 30°S after October 1991 and that northward transport may not be as strong as that observed after December 1991. To illustrate the impacts of these discrepancies on ice nucleation rates, a sensitivity test was done. We raised the injection heights of the initial Pinatubo SO_2 by ~3 km above those in our standard calculations. In this case the Pinatubo aerosol cloud remains at higher altitudes for a longer period of time, and the downward transport into the troposphere is

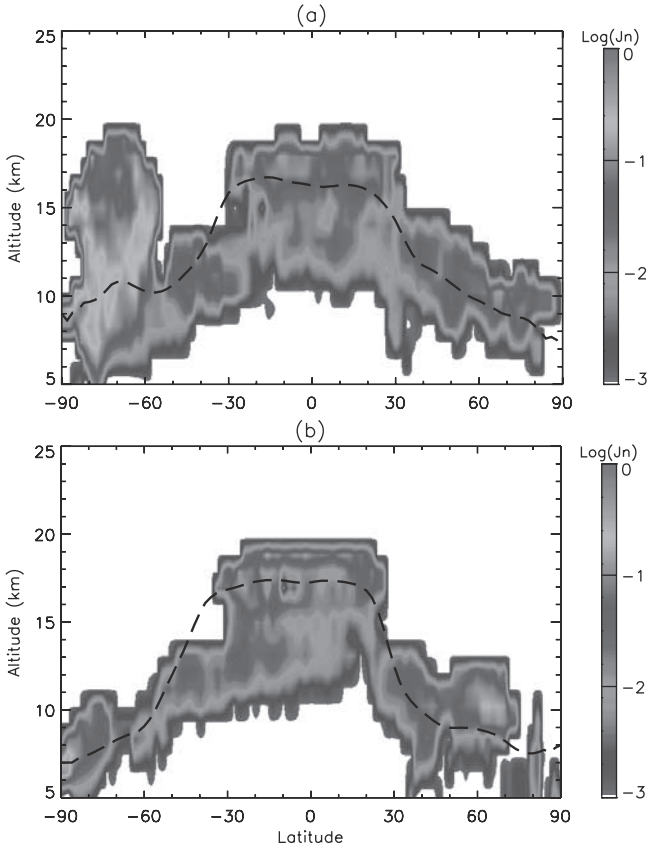

Figure 9. Same as in Figure 4 but for 1 year later for (a) 15 October 1992 and (b) 15 January 1993. A logarithmic scale is used for the homogeneous ice nucleation rates. The dashed line shows the model calculated tropopause. See color version of this figure at back of this issue.

thus smaller during the first 10 months after the eruption. However, the upper boundary of simulated aerosol layer is now 3–4 km higher than that in the observations. The global H_2SO_4 aerosol burden is increased, with the peak value in October 1991 increased from 21.7 Tg in the standard case to 23.3 Tg. This is because the transport to the tropopause takes longer and the loss of aerosols in the troposphere is smaller during the early period of the eruption in the sensitivity case. The northward transport after December 1991 is now stronger due to the larger aerosol burden. After 10 months following the eruption, when the Pinatubo aerosol cloud gradually falls down, the downward rate of transport of the Pinatubo aerosol is larger than that in the standard case. Ice nucleation rates of the Pinatubo H_2SO_4 aerosols in the Southern Hemisphere and in the region near the tropical tropopause are reduced in the sensitivity case as compared with those in the standard case during the first 10 months after the eruption. But the difference is <70%. After 10 months following the eruption the nucleation rates are generally larger than those in the standard case. However, the difference in the Northern Hemisphere and in the region near the tropical tropopause is <60% and that in the Southern Hemisphere is <20%. Thus, although there are still some discrepancies between the simulated Pinatubo aerosol distributions and observations due to some factors such as the excessive cross tropopause flux of DAO meteorological data and a relatively small nonconservation of mass, the impact on our calculated ice nucleation rates should be a factor of <2. This is a small change compared to the uncertainties involved in the parameterization of homogeneous ice nucleation processes and does not invalidate our main conclusions regarding the importance of Pinatubo aerosols relative to surface aerosols.

[27] As mentioned above, the DAO data for the time period of 1991–1992 are only available at low vertical resolution (20 sigma levels with the model top at 10 hPa), and are not adequate for the purpose of modeling the Pinatubo aerosol dispersion. The DAO data for the time period of 1997/1998 are thus used for this study. While our model results reproduce many of the dispersal features of the Pinatubo aerosol cloud, for the calculation of nucleation rates the temperature and RH_w for the 1991/1992 were also compared with values from 1997/1998. Our comparison showed that the distribution patterns of the zonal mean temperature and RH_w in 1991/1992 data are quite similar to those in 1997/1998 data (which are shown in Figures 5 and 6) for the regions with altitudes between 5 and 20 km where ice nucleation mainly takes place. We did notice that temperatures in the minimum region near the equatorial tropopause (16–18 km altitude) were higher in 1991/1992 data by $\sim$1°–3°C. The heating of the Pinatubo aerosol through the absorption of upwelling infrared radiation could explain these higher temperatures. Vertical interpolation for the purpose of comparison might also contribute to the temperature difference in this region due to the low resolution of 1991/1992 data. *Young et al.* [1994] showed that temperature perturbations produced by the Pinatubo volcanic cloud were generally 1°–4°C during the 2–3 months after the eruption in the region between 20 and 30 km altitude where the main Pinatubo plume was located. The positive temperature anomalies gradually decreased during 1992 as the tropical aerosol dispersed [*McCormick et al.*, 1995]. To further illustrate this, a model run using the DAO 1991/1992 data was performed in our study and ice nucleation rates were then calculated. Our results show that the local maxima of the zonal mean ice nucleation rates are still visible with magnitudes generally the same as those shown in Figure 4, although the vertical resolution is now much coarser. Therefore the temperature and RH_w difference between the 1991/1992 data and the 1997/1998 data could influence the calculations of ice nucleation rates; however, the magnitudes in the main Pinatubo cloud should remain the same. Furthermore, the contrast between the Pinatubo and surface aerosol nucleation rates, which are evaluated under the same temperature and RH_w, would remain similar to those presented here.

[28] It should be noted that DAO GEOS-1 reanalysis of upper tropospheric moisture has a large uncertainty because of the lack of observations and difficulty in global model simulations, which can influence the computed homogeneous freezing rate J_{ls} in this study. For example, *Starr et al.* [1995] showed that the upper tropospheric humidity in the GEOS-1 reanalysis is overestimated in the tropics and underestimated in the extratropics as compared to radiosonde observations. In the GEOS-1 GCM the moist physics uses the relaxed Arakawa-Schubert scheme (RAS) for

subgrid penetrative and shallow cumulus convection [*Moorthi and Suarez*, 1992]. RAS predicts mass fluxes from cloud types which have different entrainment rates and levels of neutral buoyancy, depending upon the properties of the large scale environment. In addition to the RAS cumulus convection scheme the GEOS-1 GCM employs a Kessler-type scheme for the re-evaporation of falling rain [*Sud and Molod*, 1988]. Supersaturation or large-scale convection is defined in the GEOS-1 GCM whenever the specific humidity in any grid box exceeds its supersaturation value with respect to water. The large-scale precipitation scheme rains at supersaturation and re-evaporates during descent to partially saturate lower layers in a process that accounts for some simple microphysics [*Takacs et al.*, 1994]. *Molod et al.* [1996] showed that RAS is constantly overadjusting the tropical atmosphere, causing a climatological dry bias in the western Pacific and South Pacific convergence zone regions, and this is corroborated by excessive GEOS-1 precipitation there. The GEOS-1 GCM parameterization of large-scale rain requires a relative humidity of 100% before the atmosphere rains out or produces clouds. Other GCMs [*Slingo and Ritter*, 1985] allow cloud formation at relative humidities <100% based on the concept that some areas of the grid box will be saturated before the grid-scale relative humidity reaches saturation. A scheme like this in a GCM will reduce the upper tropospheric moisture due to cloud formation and rain out. There are also some comparisons of upper tropospheric humidity between different reanalysis. For example, *Ho et al.* [1998] showed that, except in some high latitude regions, the zonal mean humidity difference between GEOS-1 and National Centers for Environmental Prediction/National Center for Atmospheric Research (NCEP/NCAR) is <25% and that, overall, the NCEP/NCAR humidity is higher than the GEOS-1 humidity in the lower troposphere; the reverse is true in the upper troposphere. The uncertainty in the upper tropospheric moisture will influence the computed ice nucleation rates. A lower nucleation rate may be more reasonable if the relative humidity in GEOS-1 data set is too large. However, since we calculated the ice nucleation rates of Pinatubo and surface aerosols under the same humidity, the contrast between them will not change and the main conclusions of this paper will remain the same.

[29] To check the sensitivity of the calculated homogeneous ice nucleation rates to the assumed aerosol composition, a second set of calculations for aerosols from surface sources is done by assuming that the composition of the particles is ammonium sulfate. The composition of $(NH_4)_2SO_4$ versus H_2SO_4 can influence aerosol droplet sizes through the Köhler equation due to the different interfacial surface tension of the solution-air interface, water activity, and dry particulate density under the same meteorological conditions. The equilibrium melting point depression ΔT_m and the coefficient for λ are also different for the two different compositions. However, our calculated distribution patterns for the nucleation rate of $(NH_4)_2SO_4$ aerosols are quite similar to those of H_2SO_4 aerosols. Also, absolute values differ by <50% with the local maxima of the nucleation rates of $(NH_4)_2SO_4$ aerosols higher by ~30%. The experiments by *Chen et al.* [2000] also suggested that the extent of neutralization of sulfuric acid aerosols by ammonia is unlikely to play an important role in homogeneous freezing under upper tropospheric conditions.

[30] In this section we have calculated the ice nucleation rates of Pinatubo H_2SO_4 solution aerosols under upper tropospheric and lower stratospheric conditions and compared them with those of H_2SO_4 aerosols from surface sources. To further investigate the impact of Pinatubo H_2SO_4 aerosols on cirrus cloud properties such as the number and size of ice crystals, cloud dynamics and microphysics need to be considered. To address the global impacts on cirrus cloud properties, a parameterization of homogeneous freezing has to be provided for global models for the number of ice crystals as a function of temperature, RH_w, and updraft velocity. Some studies have used detailed cloud microphysical models to investigate the sensitivity of the number of crystals to these parameters. For example, the results by *Jensen and Toon* [1992] suggested that when volcanic sulfate aerosols are transported into the upper troposphere, the effect on cirrus clouds could be an increase in the ice concentration by as much as a factor of 5. However, the inclusion of volcanic silicate aerosols, which could nucleate ice crystals at lower saturation, might actually decrease the ice concentration. Large volcanic aerosol nucleating more readily could grow and deplete the water vapor in the parcel such that the saturation never gets large enough for sulfate aerosols to freeze. However, the effect of volcanic aerosols on cirrus needs to be reassessed using a more recent parameterization of homogeneous ice freezing rate J_{ls} and measured data. *Jensen and Toon* [1994] found that the number of ice crystals that nucleate in cirrus is relatively insensitive to the number of aerosols as compared with the initial temperature and cooling rate (updraft velocity) for the background sulfate aerosol size distribution in the free troposphere. More recently, *Jensen et al.* [1998] presented similar results in the simulation of ice nucleation processes in upper tropospheric wave-clouds observed during the Subsonic Aircraft Contrail and Cloud Effects Special Study (SUCCESS) mission. Thus the processes are complicated and the changes in the number and size of ice crystals in cirrus clouds due to volcanic aerosols depend sensitively on a variety of factors. As mentioned in section 2, a single lognormal size distribution was used in the calculation of ice nucleation rates instead of the observed bimodality of Pinatubo aerosols. The evolution of the volume mean diameter for the aerosol as a function of time after the eruption was based on the study by *Russell et al.* [1996], which was estimated from a variety of measurements of the stratospheric aerosol effective radii R_{eff}. *Russell et al.* [1996] assumed a unimodal lognormal form to retrieve size distributions mainly due to the difficulty in constraining retrievals of the six parameters of a bimodal lognormal distribution. A time-dependent correction has been derived from the measured bimodal size distributions of *Goodman et al.* [1994] and has been applied to retrieved R_{eff} values for the unimodal lognormal size distribution [*Russell et al.*, 1996]. V_l, the (wet) solution droplet volume calculated using the Köhler equation, also depends very much on the RH_w. We calculated N_f in equation (7) for the bimodal size distribution of *Goodman et al.* [1994] with identical Pinatubo sulfate aerosol mass. It does indeed change N_f by ~60%. How-

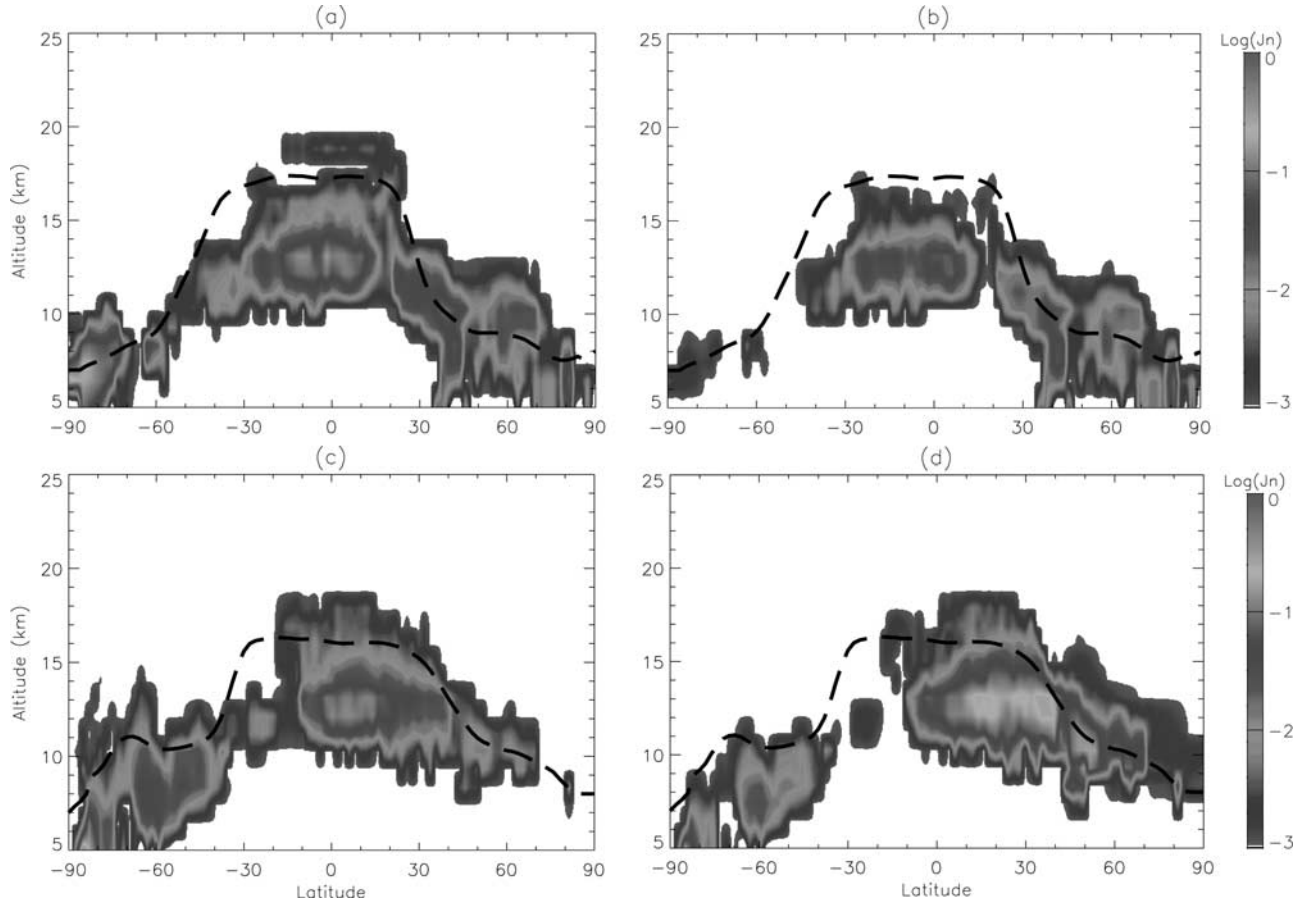

Figure 10. Latitude-altitude cross sections of the homogeneous ice nucleation rate J_n (cm^{-3} s^{-1}) of anthropogenic versus natural H_2SO_4/H_2O aerosols from surface sources in the upper troposphere and lower stratosphere. (a) Natural SO_4 in January. (b) Anthropogenic SO_4 in January. (c) Natural SO_4 in July. (d) Anthropogenic SO_4 in July. A logarithmic scale is used for the nucleation rates. See color version of this figure at back of this issue.

ever, the bimodal distribution parameters are not available as a function of time and could not be used in our study. Moreover, the uncertainty introduced by the upper tropospheric RH_w is larger than that from our use of a single unimodal distribution.

[31] The results presented above suggest that the larger and more abundant Pinatubo H_2SO_4 aerosol particles could contribute strongly to ice freezing in the upper troposphere during the first 2 years following the eruption, although the exact changes in cirrus cloud properties may depend on additional parameters. The presence of volcanic sulfate aerosols is likely to increase the frequency of cirrus clouds due to the fact that larger volcanic aerosols lower the supersaturation needed for freezing and thus freeze more readily. On the basis of NOAA polar-orbiting HIRS multispectral data, *Wylie et al.* [1994] found that a significant change in the global upper tropospheric transmissive cirrus cloud cover occurred in 1991. The frequency of cirrus occurrence increased from 35 to 43%. For the radiative effects of volcanically altered cirrus, *Minnis et al.* [1993] found increased solar scattering for optically thick clouds during the initial Pinatubo posteruption period based on the analysis of the ERBE irradiance observations. For optically thinner, high-altitude clouds with cloud effective radius <0.8 μm, measured by the SAGE series of satellite instruments, the occurrence of clouds having high extinction coefficients was suppressed, while that of clouds having low extinction coefficients was enhanced due to the Mount El Chichon volcanic aerosols [*Wang et al.*, 1995].

[32] It is also interesting to compare the ice nucleation rates of anthropogenic versus natural H_2SO_4 aerosols from surface sources. Figure 10 shows the zonal mean ice nucleation rate of H_2SO_4 aerosols from surface anthropogenic and natural sources for two seasons (winter and summer) in the upper troposphere and lower stratosphere. From Figures 10a and 10b in January we can see a larger nucleation rate of anthropogenic H_2SO_4 aerosols north of 30°S, while that of natural aerosols is more widely spread. During this season of the year, anthropogenic activities produce relatively fewer sulfate aerosols than in other seasons. Thus the nucleation rate of anthropogenic H_2SO_4 aerosols is generally smaller but still comparable in the northern midlatitudes to that from the natural sources. In July, when the production of anthropogenic sulfate is much stronger in the Northern Hemisphere, the nucleation rate of H_2SO_4 aerosols from anthropogenic sources dominates in the regions of the Northern Hemisphere, especially between 10° and 50°N. Therefore anthropogenic sulfate could have

disturbed and influenced ice nucleation rates and possibly cirrus properties in the upper troposphere.

4. Summary and Conclusions

[33] In this work, a 2-year simulation of the Mount Pinatubo volcanic aerosol with a global chemistry and transport model was described. The model is driven by meteorological fields from the NASA Goddard Data Assimilation Office general circulation model. The model reproduces many of the dispersal characteristics of the Pinatubo aerosol cloud after the eruption as determined from satellite measurements. The simulated latitude-altitude cross sections of Pinatubo aerosol extinction ratio are quite similar to those of *Trepte et al.* [1993] derived from the SAGE II data.

[34] On the the basis of simulated global distributions of Pinatubo sulfate, the homogeneous ice nucleation rate of Pinatubo H_2SO_4 aerosol in the lower stratosphere and upper troposphere is calculated and compared with that of natural and anthropogenic sulfate from Earth's surface sources. Strong ice nucleation rates of the Pinatubo H_2SO_4 aerosol are found in the region around the equatorial tropopause and also in regions along the tropopause near the bottom of the main Pinatubo cloud layer during the 1–2 years after the eruption. High nucleation rates are also found in the southern extratropical regions in the altitudes between 5 and 20 km during the summer and autumn, due to the lower temperature and high RH_w occurring there. The ice nucleation rates of Mount Pinatubo sulfate are larger than those of sulfate from surface sources in many regions of the upper troposphere during the first year of the eruption and could be still comparable in the second year after the eruption.

[35] Our calculated ice nucleation rates depend on many factors: the simulated global distribution of sulfate mass mixing ratio, the Pinatubo aerosol size distribution, meteorological parameters (temperature and RH_w), and the homogeneous freezing parameterization and related parameters. Considering the uncertainties involved in these factors, our calculation of ice nucleation rate of Pinatubo sulfate aerosol is still preliminary. However, our results suggest that the Pinatubo volcanic eruption could have influenced cirrus formation and evolution globally through the homogeneous freezing of H_2SO_4 aerosol as compared to sulfate from the surface sources at least for the first 2 years after the eruption. Available satellite observations support this assertion.

[36] **Acknowledgments.** We thank the NASA Atmospheric Effects of Aviation Program as well as the DOE Atmospheric Chemistry Program for partial funding of this work. Cynthia Atherton, Daniel Bergmann, and John Tannahill of Lawrence Livermore National Laboratory provided assistance in using and updating the LLNL/IMPACT model.

References

Balkanski, Y. J., D. J. Jacob, G. M. Gardner, W. M. Graustein, and K. K. Turekian, Transport and residence times of continental aerosols inferred from a global 3-dimensional simulation of 210 Pb, *J. Geophys. Res.*, *98*, 20,573–20,586, 1993.

Bertram, A. K., D. D. Patterson, and J. J. Sloan, Mechanisms and temperatures for the freezing of sulfuric acid aerosols measured by FTIR extinction spectroscopy, *J. Phys. Chem.*, *100*, 2376–2383, 1996.

Bluth, G. J. S., S. D. Doiron, C. C. Schnetzler, A. J. Krueger, and L. S. Walter, Global tracking of the SO_2 clouds from the June 1991 Mount Pinatubo eruptions, *Geophys. Res. Lett.*, *19*, 151–154, 1992.

Chen, J. P., Theory of deliquescence and modified Köhler curves, *J. Atmos. Sci.*, *51*, 3505–3516, 1994.

Chen, Y., P. J. DeMott, S. M. Kreidenweis, D. C. Rogers, and D. E. Sherman, Ice fromation by sulfate and sulfuric acid aerosol particles under upper-tropospheric conditions, *J. Atmos. Sci.*, *57*, 3752–3766, 2000.

Choi, W., W. B. Grant, J. H. Park, K.-M. Lee, H. Lee, and J. M. Russell III, Role of the quasi-biennial oscillation in the transport of aerosols from the tropical stratospheric reservoir to midlatitudes, *J. Geophys. Res.*, *103*, 6033–6042, 1998.

Chuang, C. C., J. E. Penner, K. E. Grant, J. M. Prospero, and G. H. Rau, Cloud susceptibility and the first aerosol indirect forcing: Sensitivity to black carbon and aerosol concentrations, *J. Geophys. Res.*, in press, 2002.

Clegg, S. L., and P. Brimblecombe, Application of a multicomponent thermodynamic model to activities and thermal properties of 0–40 mol kg^{-1} aqueous sulfuric acid from <200 to 328 K, *J. Chem. Eng. Data*, *40*, 43–64, 1995.

DeMott, P. J., M. P. Meyers, and W. R. Cotton, Numerical model simulations of cirrus clouds including homogeneous and heterogeneous ice nucleation, *J. Atmos. Sci.*, *51*, 77–90, 1994.

DeMott, P. J., D. C. Rogers, and S. M. Kreidenweis, The susceptibility of ice formation in upper tropospheric clouds to insoluble aerosol components, *J. Geophys. Res.*, *102*, 19,575–19,584, 1997.

Deshler, T., D. J. Hofmann, B. J. Johnson, and W. R. Rozier, Bolloonborne measurements of the Pinatubo aerosol size distribution and volatility at Laramie, Wyoming, during the summer of 1991, *Geophys. Res. Lett.*, *19*, 199–202, 1992.

Deshler, T., B. J. Johnson, and W. R. Rozier, Balloonborne measurements of Pinatubo aerosol during 1991 and 1992 at 41°N: Vertical profiles, size distributions, and volatility, *Geophys. Res. Lett.*, *20*, 1435–1438, 1993.

Fitzgerald, J. W., Effects of aerosol composition on cloud droplet size distribution: A numerical study, *J. Atmos. Sci.*, *31*, 1358–1367, 1974.

Giorgi, F., and W. L. Chameides, Rainout lifetimes of highly soluble aerosols and gases as inferred from simulations with a general circulation model, *J. Geophys. Res.*, *91*, 14,367–14,376, 1986.

Goodman, J., K. G. Snetsinger, R. F. Pueschel, G. V. Ferry, and S. Verma, Evolution of Pinatubo aerosol near 19 km altitude over western North America, *Geophys. Res. Lett.*, *21*, 1129–1132, 1994.

Grant, W. B., E. V. Browell, C. S. Long, L. L. Stowe, R. G. Grainger, and A. Lambert, Use of volcanic aerosols to study the tropical stratospheric reservoir, *J. Geophys. Res.*, *101*, 3973–3988, 1996.

Guasta, M. D., M. Morandi, L. Stefanutti, B. Stein, J. Kolenda, P. Rairoux, J. P. Wolf, R. Matthey, and E. Kyro, Multiwavelength lidar observation of thin cirrus at the base of the Pinatubo stratospheric layer during the EASOE campaign, *Geophys. Res. Lett.*, *21*, 1339–1342, 1994.

Heymsfield, A. J., and R. M. Sabin, Cirrus crystal nucleation by homogeneous freezing of solution droplets, *J. Atmos. Sci.*, *46*, 2252–2264, 1989.

Hitchman, M. H., M. Mckay, and C. R. Trepte, A climatology of stratospheric aerosol, *J. Geophys. Res.*, *99*, 20,689–20,700, 1994.

Ho, C.-H., M.-D. Chou, M. Suarez, K.-M. Lau, and M. M.-H. Yan, Comparison of model-calculated and ERBE-retrieved clear-sky outgoing longwave radiation, *J. Geophys. Res.*, *103*, 11,529–11,536, 1998.

Hofmann, D. J., and S. J. Oltmans, Anomalous Antarctic ozone during 1992: Evidence for Pinatubo volcanic aerosol effects, *J. Geophys. Res.*, *98*, 18,555–18,561, 1993.

Hofmann, D. J., S. J. Oltmans, J. A. Lathrop, J. M. Harris, and H. Vomel, Record low ozone at the South Pole in the spring of 1993, *Geophys. Res. Lett.*, *21*, 421–424, 1994.

Jacob, D. J., and S. C. Wofsy, Budgets of reactive nitrogen, hydrocarbons, and ozone over the Amazon forest during the wet season, *J. Geophys. Res.*, *95*, 16,737–16,754, 1990.

Jensen, E. J., and O. B. Toon, The potential effects of volcanic aerosols on cirrus cloud microphysics, *Geophys. Res. Lett.*, *19*, 1759–1762, 1992.

Jensen, E. J., and O. B. Toon, Ice nucleation in the upper troposphere: Sensitivity to aerosol number density, temperature, and cooling rate, *Geophys. Res. Lett.*, *21*, 2019–2022, 1994.

Jensen, E. J., O. B. Toon, and P. Hamill, Homogeneous freezing nucleation of stratospheric solution droplets, *Geophys. Res. Lett.*, *18*, 1857–1860, 1991.

Jensen, E. J., O. B. Toon, D. L. Westphal, S. Kinne, and A. J. Heymsfield, Microphysical modeling of cirrus, 1, Comparison with 1986 FIRE IFO measurements, *J. Geophys. Res.*, *99*, 10,421–10,442, 1994.

Jensen, E. J., et al., Ice nucleation processes in upper tropospheric wave-clouds observed during SUCCESS, *Geophys. Res. Lett.*, *25*, 1363–1366, 1998.

Juckes, M. N., and M. E. McIntyre, A high resolution, one-layer model of breaking planetary waves in the winter stratosphere, *Nature*, *328*, 590–596, 1987.

Koop, T. H., H. P. Ng, L. T. Molina, and M. J. Molina, A new optical technique to study aerosol phase transitions: The nucleation of ice from H_2SO_4 aerosol, *J. Phys. Chem. A*, *102*, 8924–8931, 1998.

Krueger, A. J., L. S. Walter, P. K. Bhartia, C. C. Schnetzler, N. A. Krotkov, I. Sprod, and G. J. S. Bluth, Volcanic sulfur dioxide measurements from the total ozone mapping spectrometer instruments, *J. Geophys. Res.*, *100*, 14,057–14,076, 1995.

Lambert, A., R. G. Grainger, C. D. Rodgers, F. W. Taylor, J. L. Mergenthaler, J. B. Kumer, and S. T. Massie, Global evolution of the Mt. Pinatubo volcanic aerosols observed by the infrared limb-sounding instruments CLAES and ISAMS on the Upper Atmosphere Research Satellite, *J. Geophys. Res.*, *102*, 1495–1512, 1997.

Larson, N., The impact of freezing of sulfate aerosols on the formation of polar stratospheric clouds, *Geophys. Res. Lett.*, *21*, 425–428, 1994.

Lin, S.-J., and R. B. Rood, Multidimensional flux-form semi-Lagrangian transport schemes, *Mon. Weather Rev.*, *124*, 2046–2070, 1996.

Liou, K. N., Influence of cirrus clouds on weather and climate processes: A global perspective, *Mon. Weather Rev.*, *114*, 1167–1199, 1986.

McCormick, M. P., and R. E. Veiga, SAGE II measurements of early Pinatubo aerosols, *Geophys. Res. Lett.*, *19*, 155–158, 1992.

McCormick, M. P., C. R. Trepte, and G. S. Kent, Spatial changes in the stratospheric aerosol associated with the north polar vortex, *Geophys. Res. Lett.*, *10*, 941–944, 1983.

McCormick, M. P., L. W. Thomason, and C. R. Trepte, Atmospheric effects of the Mt. Pinatubo eruption, *Nature*, *373*, 399–404, 1995.

Minnis, P., E. F. Harrison, L. L. Stowe, G. G. Gibson, F. M. Denn, D. R. Doelling, and W. L. Smith Jr., Radiative climate forcing by the Mount Pinatubo Eruption, *Science*, *259*, 1411–1415, 1993.

Mitchel, J. F. B., C. A. Senior, and W. J. Ingram, CO_2 and climate: A missing feedback?, *Nature*, *341*, 132–134, 1988.

Molod, A., H. M. Helfand, and L. L. Takacs, The climatology of parameterized physical processes in the GEOS-1 GCM and their impact on the GEOS-1 data assimilation system, *J. Clim.*, *9*, 764–785, 1996.

Moorthi, S., and M. J. Suarez, Relaxed Arakawa-Schubert: A parameterization of moist convection for general circulation models, *Mon. Weather Rev.*, *120*, 978–1002, 1992.

Osborn, M. T., R. J. DeCoursey, C. R. Trepte, D. M. Winker, and D. C. Woods, Evolution of the Pinatubo volcanic cloud over Hampton, Virginia, *Geophys. Res. Lett.*, *22*, 1101–1104, 1995.

Penner, J. E., C. A. Atherton, J. Dignon, S. J. Ghan, J. J. Walton, and S. Hameed, Tropospheric nitrogen: A three-dimensional study of sources, distribution, and deposition, *J. Geophys. Res.*, *96*, 959–990, 1991.

Penner, J. E., C. A. Atherton, and T. E. Graedel, Global emissions and models of photochemically active compounds, in *Global Atmospheric-Biospheric Chemistry*, edited by R. Prinn, pp. 223–248, Plenum, New York, 1994.

Penner, J. E., D. J. Bergmann, J. J. Walton, D. Kinnison, M. J. Prather, D. Rotman, C. Price, K. E. Pickering, and S. L. Baughcum, An evaluation of upper troposphere NO_x with two models, *J. Geophys. Res.*, *103*, 22,097–22,113, 1998.

Penner, J. E., et al., Aerosols: Their direct and indirect effects, in *Intergovernmental Panel on Climate Change, Report to IPCC from the Scientific Assessment Working Group*, in press, 2001.

Pruppacher, H. R., and J. D. Klett, *Microphysics of Cloud and Precipitation*, 954 pp., Dordrecht, 1997.

Pueschel, R. F., J. M. Livingston, P. B. Russell, and S. Verma, Physical and optical properties of the Pinatubo volcanic aerosol: Aircraft observations with impactors and a suntracking photometer, *J. Geophys. Res.*, *99*, 12,915–12,922, 1994a.

Pueschel, R. F., J. M. Livingston, G. V. Ferry, and T. E. DeFelice, Aerosol abundances and optical characteristics in the Pacific Basin free troposphere, *Atmos. Environ.*, *28*, 951–960, 1994b.

Ramanathan, V., E. J. Pitcher, R. C. Malone, and M. L. Blackmon, The response of a spectral general circulation model to refinements in radiative processes, *J. Atmos. Sci.*, *40*, 605–630, 1983.

Rard, J. A., A. Habenschuss, and F. H. Spedding, A review of the osmotic coefficients of aqueous H_2SO_4 at 25°C, *J. Chem. Eng. Data*, *21*, 374–379, 1976.

Read, W. G., L. Froidevaux, and J. W. Waters, Microwave limb sounder measurements of stratospheric SO_2 from the Mt. Pinatubo volcano, *Geophys. Res. Lett.*, *20*, 1299–1302, 1993.

Rind, D., and X. Liao, Stratospheric Aerosol and Gas Experiment II CD-ROM atlas of global monthly mean aerosols, ozone, NO_2, water vapor, and relative humidity (1985–1993), *Earth Interact.*, *1*, 1997. (Available at http://EarthInteractions.org)

Russell, P. B., et al., Satellite and correlative measurements of the stratospheric aerosol, II, Comparison of measurements made by SAM-2, dustsondes, and an airborne lidar, *J. Atmos. Sci.*, *38*, 1295–1312, 1981.

Russell, P. B., et al., Global to microscale evolution of the Pinatubo volcanic aerosol derived from diverse measurements and analyses, *J. Geophys. Res.*, *101*, 18,745–18,763, 1996.

Sassen, K., Evidence for liquid-phase cirrus clouds formation from volcanic aerosols: Climate implications, *Science*, *257*, 516–519, 1992.

Sassen, K., and S. Benson, Ice nucleation in cirrus clouds: A model study of the homogeneous and heterogeneous modes, *Geophys. Res. Lett.*, *27*, 521–524, 2000.

Sassen, K., and G. C. Dodd, Homogeneous nucleation rate for highly supercooled cirrus cloud droplets, *J. Atmos. Sci.*, *45*, 1357–1369, 1988.

Sassen, K., D. O. C. Starr, G. G. Mace, M. R. Poellot, S. H. Melfi, W. L. Eberhard, J. D. Spinhirne, E. W. Eloranta, D. E. Hagen, and J. Hallett, The 5–6 December 1991 FIRE IFO II jet stream cirrus case study: Possible influences of volcanic aerosols, *J. Atmos. Sci.*, *52*, 97–123, 1995.

Seinfeld, J. H., and S. N. Pandis, *Atmospheric Chemistry and Physics: From Air Pollution to Climate Change*, John Wiley, New York, 1998.

Slingo, J., and B. Ritter, Cloud prediction in the ECMWF model, *Tech. Rep. 46*, Eur. Cent. for Medium-Range Weather Forecasts, Reading, UK, 1985.

Starr, D. O. C., B. C. Diehl, A. R. Lare, and B. J. Soden, Upper tropospheric humidity in the 5-year GEOS assimilation, in *Proceedings of the Workshop on the GEOS-1 Five-Year Assimilation,* vol. 7, *NASA Tech. Memo. 104606*, pp. 75–79, NASA, Washington, D.C., 1995.

Steele, H. M., and P. Hamill, Effects of temperature and humidity on the growth and optical properties of sulfuric acid-water droplets, *J. Aerosol Sci.*, *12*, 517–528, 1981.

Stowe, L. L., R. M. Carey, and P. P. Pellegrino, Monitoring the Mt. Pinatubo aerosol layer with NOAA/11 AVHRR data, *Geophys. Res. Lett.*, *19*, 159–162, 1992.

Sud, Y. C., and A. Molod, The role of dry convection, cloud-radiation feedback processes and the influence of recent improvements in the parameterization of convection in the GLA GCM, *Mon. Weather Rev.*, *116*, 2366–2387, 1988.

Tabazadeh, A., O. B. Toon, S. L. Clegg, and P. Hamill, A new parameterization of H_2SO_4/H_2O aerosol composition: Atmospheric implications, *Geophys. Res. Lett.*, *24*, 1931–1934, 1997.

Takacs, L. L., A. Molod, and T. Wang, Documentation of the Goddard Earth Observation System (GEOS) general circulation model, version 1, *NASA Tech. Memo. 104606,* vol. 1, NASA, Washington, D.C., 1994.

Timmreck, C., H.-F. Graf, and I. Kirchner, A one-and-half-year interactive MA/ECHAM4 simulation of Mount Pinatubo aerosol, *J. Geophys. Res.*, *104*, 9337–9359, 1999.

Trepte, C. R., and M. H. Hitchman, Tropical stratospheric circulation deduced from satellite aerosol data, *Nature*, *355*, 626–628, 1992.

Trepte, C. R., R. E. Veiga, and M. P. McCormick, The poleward dispersal of Mount Pinatubo volcanic aerosol, *J. Geophys. Res.*, *98*, 18,563–18,573, 1993.

Trepte, C. R., L. W. Thomason, and G. S. Kent, Banded structures in stratospheric aerosol distributions, *Geophys. Res. Lett.*, *21*, 2397–2400, 1994.

Walcek, C. J., R. A. Brost, J. S. Chang, and M. L. Wesely, SO_2, sulfate, and HNO_3 deposition velocities computed using regional landuse and meteorological data, *Atmos. Environ.*, *20*, 949–964, 1986.

Wang, P. H., P. Minnis, and G. K. Yue, Extinction coefficient (1 μm) properties of high-altitude clouds from solar occultation measurements (1985–1990): Evidence of volcanic aerosol effect, *J. Geophys. Res.*, *100*, 3181–3199, 1995.

Wesely, M. L., Parameterization of surface resistances to gaseous dry deposition in regional-scale numerical models, *Atmos. Environ.*, *23*, 1293–1304, 1989.

Wylie, D. P., W. P. Menzel, H. M. Woolf, and K. I. Strabala, Four years of global cirrus cloud statistics using HIRS, *J. Clim.*, *7*, 1972–1986, 1994.

Young, R. E., H. Houben, and O. B. Toon, Radiatively formed dispersion of the Mt. Pinatubo volcanic cloud and induced temperature perturbations in the stratosphere during the first few months following the eruption, *Geophys. Res. Lett.*, *21*, 369–372, 1994.

Yue, G. K., L. R. Poole, P.-H. Wang, and E. W. Chiou, Stratospheric aerosol acidity, density, and refractive index deduced from SAGE II and NMC temperature data, *J. Geophys. Res.*, *99*, 3727–3787, 1994.

X. Liu and J. E. Penner, Department of Atmospheric, Oceanic and Space Sciences, University of Michigan, 2455 Hayward, Ann Arbor, MI 48109-1349, USA. (xhliu@engin.umich.edu; penner@tumich.edu)

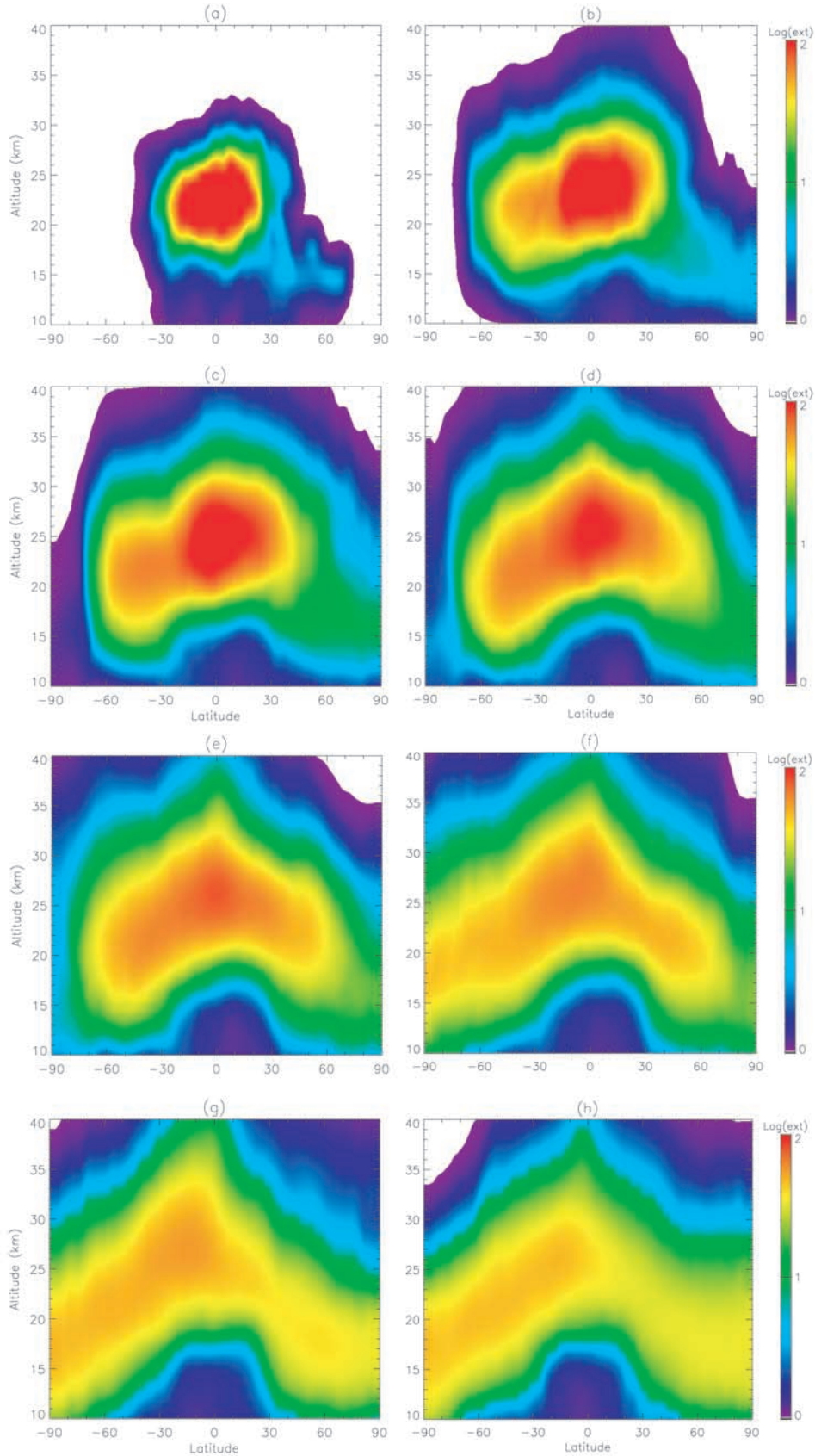

Figure 2. Latitude-altitude cross sections of the extinction ratio for (a) 15 July 1991, (b) 15 August 1991, (c) 15 September 1991, (d) 15 October 1991, (e) 15 November 1991, (f) 15 December 1991, (g) 15 February 1992, and (h) 15 April 1992. A logarithmic scale is used for the extinction ratio.

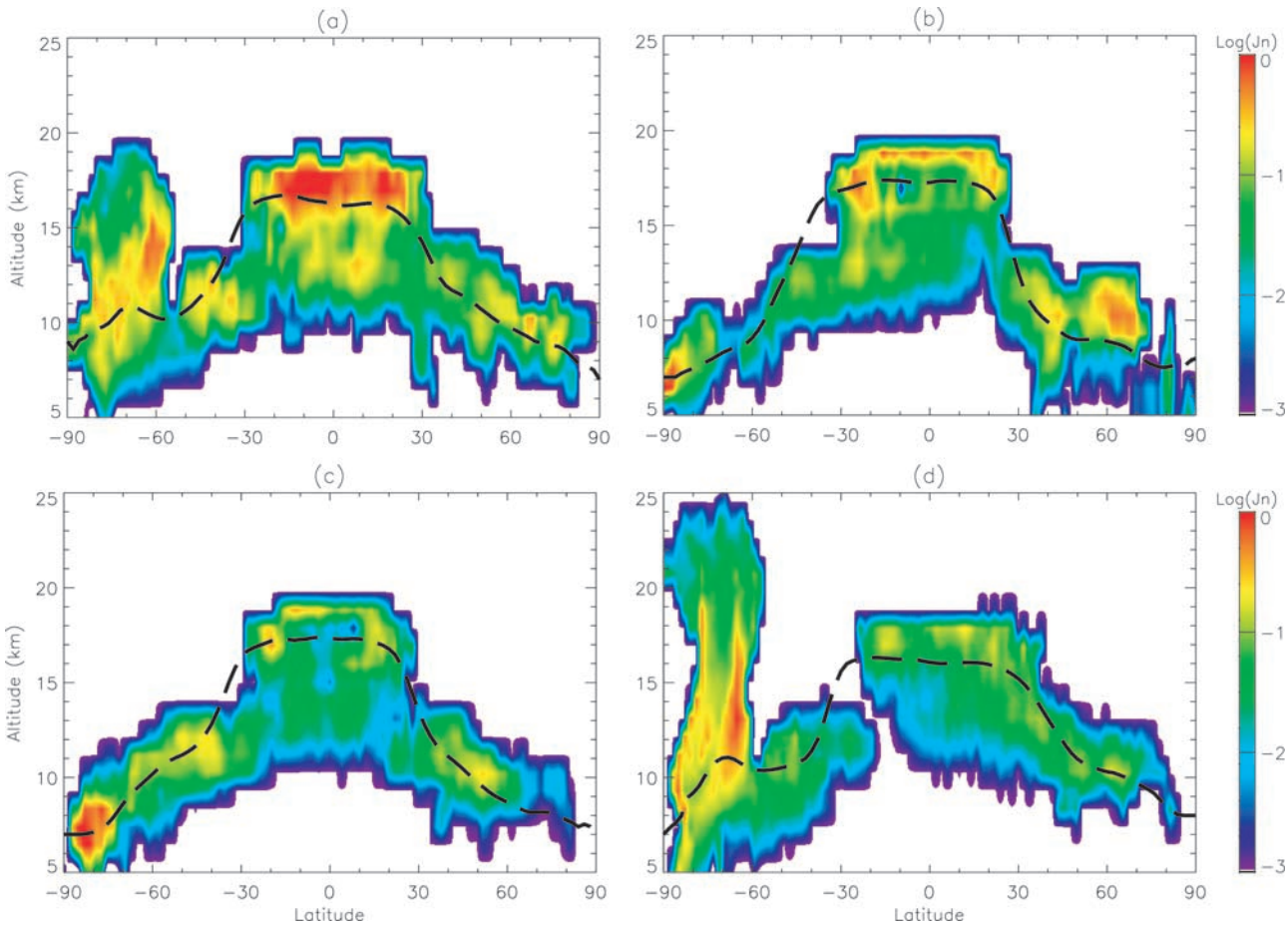

Figure 4. Latitude-altitude cross sections of the homogeneous ice nucleation rate J_n (cm^{-3} s^{-1}) of Mount Pinatubo H_2SO_4/H_2O particles as a function of post-Pinatubo time for (a) 15 October 1991, (b) 15 January 1992, (c) 15 April 1992, and (d) 15 July 1992. A logarithmic scale is used for the nucleation rates. The dashed line shows the model calculated tropopause.

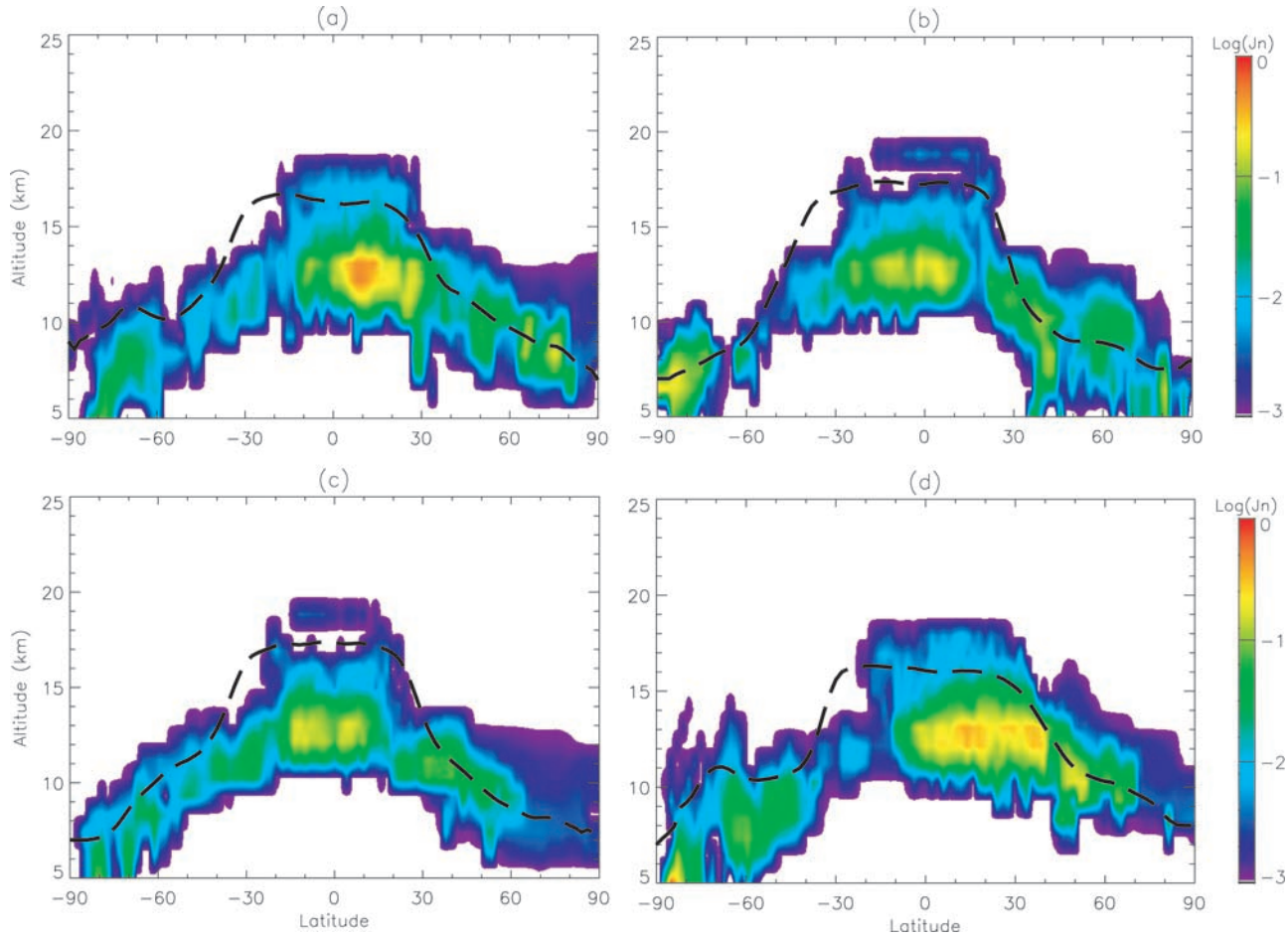

Figure 8. Latitude-altitude cross sections of the homogeneous ice nucleation rate J_n (cm^{-3} s^{-1}) of H_2SO_4/H_2O particles from surface sources (anthropogenic plus natural) in the upper troposphere and lower stratosphere in (a) October, (b) January, (c) April, and (d) July. A logarithmic scale is used for the nucleation rates.

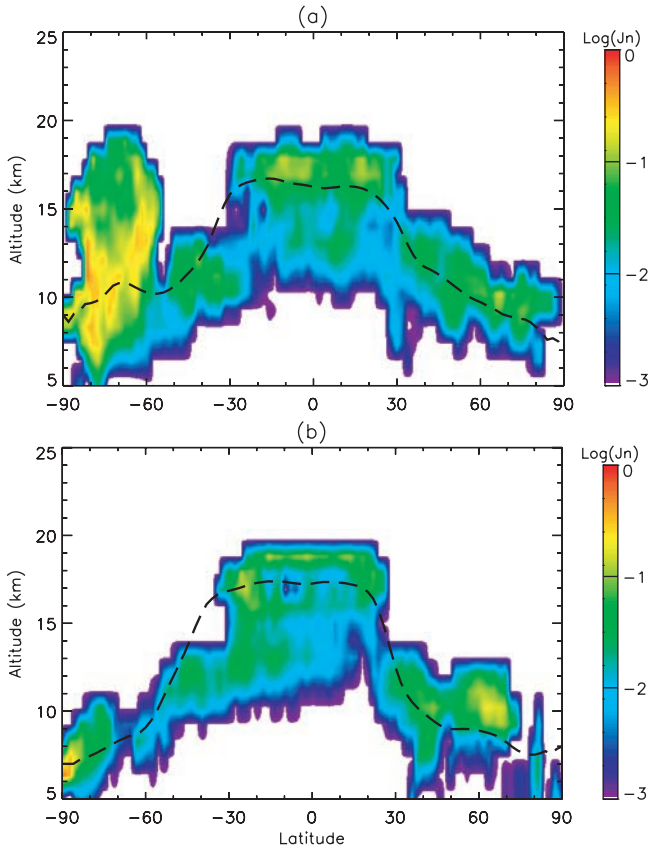

Figure 9. Same as in Figure 4 but for 1 year later for (a) 15 October 1992 and (b) 15 January 1993. A logarithmic scale is used for the homogeneous ice nucleation rates. The dashed line shows the model calculated tropopause.

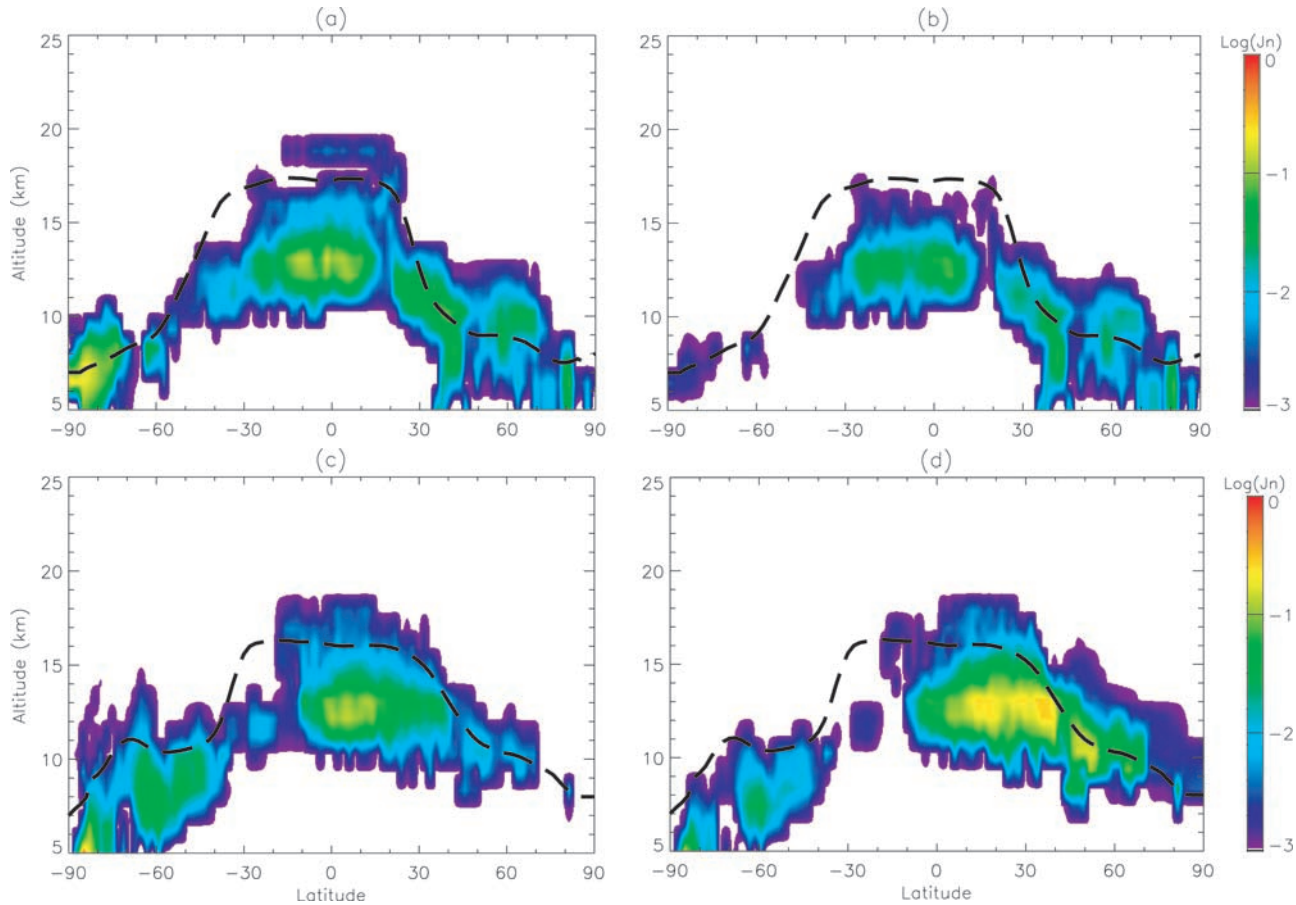

Figure 10. Latitude-altitude cross sections of the homogeneous ice nucleation rate J_n (cm^{-3} s^{-1}) of anthropogenic versus natural H_2SO_4/H_2O aerosols from surface sources in the upper troposphere and lower stratosphere. (a) Natural SO_4 in January. (b) Anthropogenic SO_4 in January. (c) Natural SO_4 in July. (d) Anthropogenic SO_4 in July. A logarithmic scale is used for the nucleation rates.